



1 Volatile Oxidation Products and Secondary Organosiloxane Aerosol 2 from D₅ + OH at Varying OH Exposures

3 Hyun Gu Kang¹, Yanfang Chen², Jiwoo Jeong², Yoojin Park³, Thomas Berkemeier¹, Hwajin Kim^{2,4}

4 ¹Multiphase Chemistry Department, Max Planck Institute for Chemistry, 55128 Mainz, Germany

5 ²Department of Environmental Health Sciences, Graduate School of Public Health, Seoul National University, 08826 Seoul,
6 South Korea

7 ³Department of Environmental Science and Engineering, College of Engineering, Ewha Womans University, 03760 Seoul,
8 South Korea

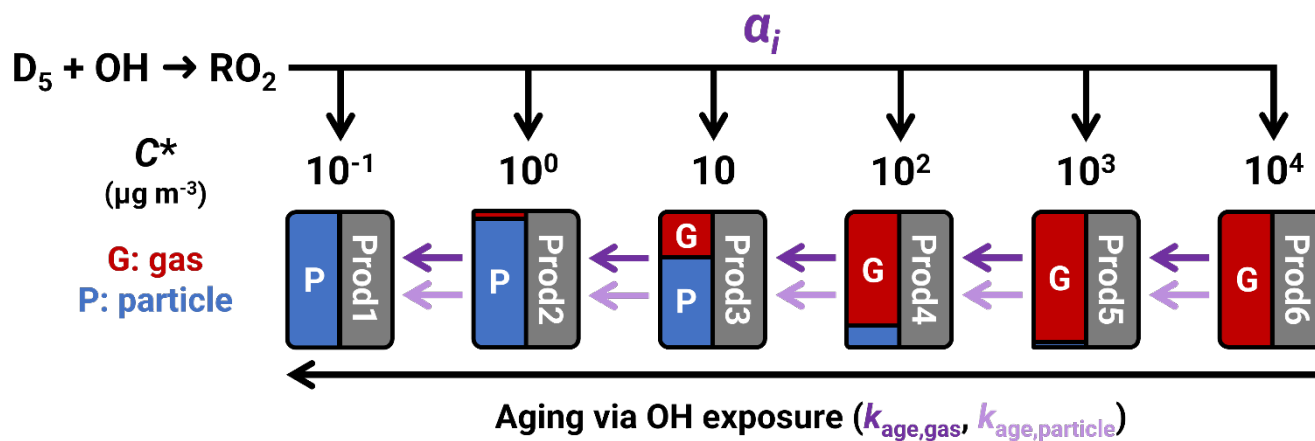
9 ⁴Institute of Health and Environment, Graduate School of Public Health, Seoul National University, 08826 Seoul, South
10 Korea

11 *Correspondence to:* Hwajin Kim (khj0116@snu.ac.kr) and Thomas Berkemeier (t.berkemeier@mpic.de)

12 **Abstract.** Siloxanes are composed of silicon, oxygen, and alkyl groups and are emitted from consumer chemicals. Despite
13 being entirely anthropogenic, siloxanes are being detected in remote regions and are ubiquitous in indoor and urban
14 environments. Decamethylcyclopentasiloxane (D₅) is one of the most common cyclic congeners, and smog chamber and
15 oxidation flow reactor (OFR) experiments have found D₅ + OH to form secondary organosiloxane aerosol (SOSiA). However,
16 there is uncertainty about the reaction products, and the reported SOSiA mass yields (Y_{SOSiA}) appear inconsistent. To quantify
17 small volatile oxidation products (VOP) and to consolidate the Y_{SOSiA} in the literature, we performed experiments using a
18 Potential Aerosol Mass OFR while varying D₅ concentration, humidity, and OH exposure (OH_{exp}). We use a proton transfer
19 reaction time-of-flight mass spectrometer to quantify D₅, HCHO, and HCOOH, and detect other VOP, which we tentatively
20 identify as siloxanols and siloxanyl formates. We determine molar yields of HCHO and HCOOH between 52 – 211 % and 45
21 – 127 %, respectively. With particle size distributions measured with a scanning mobility particle sizer, we find Y_{SOSiA} to be <
22 10 % at $\text{OH}_{\text{exp}} < 1.3 \times 10^{11} \text{ s cm}^{-3}$ and ~20 % at OH_{exp} corresponding to that of the lifetime of D₅ at atmospheric OH
23 concentrations. We also find that Y_{SOSiA} is dependent on both organic aerosol mass loading and OH_{exp} . We use a kinetic box
24 model of SOSiA formation and aging (aging-VBS model) to reconcile the Y_{SOSiA} values found in this study and the literature.
25 The model uses a volatility basis set (VBS) of the primary oxidation products as well as an aging rate coefficient in the gas
26 phase, $k_{\text{age,gas}}$, of $2.17 \times 10^{-11} \text{ cm}^3 \text{ s}^{-1}$, and an aging rate coefficient in the particle phase, $k_{\text{age,particle}}$, which is ten times smaller.
27 The combination of primary VBS and OH-dependent oxidative aging predicts SOSiA formation much better than a standard-
28 VBS parameterization that does not consider aging ($R^2 = 0.970$ vs. 0.847). The need for an ageing-dependent parameterization
29 to accurately model SOSiA formation shows that concepts developed for secondary organic aerosol precursors, which are able
30 to form low-volatile products at low OH_{exp} , do not necessarily apply to D₅ + OH. The resulting yields of HCHO and HCOOH
31 and the parameterization of Y_{SOSiA} may be used in larger scale models to assess the implications of siloxanes on air quality.

32

33 **Keywords:** D₅ siloxane, organic aerosol, proton transfer reaction mass spectrometer, oxidation flow reactor, chemical kinetics



34

35 **Graphical Abstract:** Schematic of the kinetic box model.

36

37

38

39

40

41

42

43

44

45

46

47

48

49

50

51

52

53



54 1 Introduction

55 Organosiloxanes are molecules composed of silicon-oxygen bonds with alkyl groups on the silicons and encompass linear and
56 cyclic species, some of which have vapor pressures on par with volatile organic compounds (VOC). Siloxanes are entirely
57 anthropogenic pollutants (Rücker and Kümmerer, 2015) commonly used in consumer and industrial chemical products (Seltzer
58 et al., 2021a; Gkatzelis et al., 2021) and their emissions are projected to increase in the coming decades (Tansel and Surita,
59 2017). Decamethylcyclopentasiloxane (D₅, C₁₀H₃₀O₅Si₅), where “D” refers to units of (CH₃)₂SiO, is a ubiquitous cyclosiloxane
60 in the ambient environment.

61

62 Siloxanes can be detected in the indoor environment (Tang et al., 2015; Tran and Kannan, 2015; Arata et al., 2021; Katz et al.,
63 2021; Kaikiti et al., 2022; Wang et al., 2022), near landfills (Schweigkofler and Niessner, 1999), and sewage treatment sites
64 (Lee et al., 2014; Horii et al., 2019). Siloxanes are also found in outdoor urban air (Xiang et al., 2021), and organosilicon
65 compounds have been found in varying amounts in ambient particulates in China (Lu et al., 2019; Cheng et al., 2021; Meng
66 et al., 2021; Song et al., 2022; Xu et al., 2022) and the United States (Milani et al., 2021).

67

68 Siloxanes are suspected to be environmentally persistent or “pseudo persistent” (Howard and Muir, 2010; Xiang et al., 2021),
69 but this long-lifetime assessment is disputed (Graiver et al., 2003; Whelan and Kim, 2021). Reaction rate coefficients of D₅
70 with atmospheric oxidants have been reported, and Atkinson (1991) found D₅ to be effectively unreactive with atmospheric
71 concentrations of O₃ ($k_{D_5+O_3} < 3 \times 10^{-20} \text{ cm}^3 \text{ s}^{-1}$) and NO₃ radicals ($k_{D_5+NO_3} < 3 \times 10^{-16} \text{ cm}^3 \text{ s}^{-1}$) at ~298 K. While D₅ is reactive
72 with OH and Cl, Alton and Browne (2020) calculated that the removal of D₅ by Cl radicals would only be a few percent of
73 that by OH radicals at typical ambient oxidant concentrations.

74

75 Atkinson (1991), Safron et al. (2015), Xiao et al. (2015), Kim and Xu (2017), and Alton and Browne (2020) have measured
76 k_{D_5+OH} at ~298 K to be 1.55×10^{-12} , 2.6×10^{-12} , 2.46×10^{-12} , 1.46×10^{-12} , and $2.1 \times 10^{-12} \text{ cm}^3 \text{ s}^{-1}$, respectively. These
77 measurements are summarized in Table S1. Xiao et al. (2015) derived k_{D_5+OH} computationally as $2.90 \times 10^{-12} \text{ cm}^3 \text{ s}^{-1}$. In this
78 paper, we use $k_{D_5+OH} = 2.0 \times 10^{-12} \text{ cm}^3 \text{ s}^{-1}$, which is a rounded average of the empirically determined rate coefficients. This
79 k_{D_5+OH} corresponds to a D₅ atmospheric lifetime of ~4 days via removal by OH, assuming a daily average OH concentration
80 ($[OH]_{\text{avg}}$) of $1.5 \times 10^6 \text{ cm}^{-3}$.

81

82 D₅ is expected to suppress O₃ formation in urban environments. Carter et al. (1993) performed a series of chamber experiments
83 mimicking urban air conditions and found that D₅ siloxane would inhibit ozone formation by suppressing the OH radical. In
84 contrast, formaldehyde (HCHO) is known to contribute to O₃ formation (Derwent et al., 1996). Fu et al. (2020) predicted the
85 formation of HCHO as a product of D₅ + OH at low NO/HO₂ conditions using quantum chemical calculations and kinetics
86 modelling, but an experimental yield of HCHO from D₅ + OH has not been reported. Atkinson (1991) proposed HCHO as a



87 product of the siloxane alkoxy radical (RO) pathway, assuming an analogous mechanism to that of VOC. Sommerlade et al.
88 (1993) suggested that HCHO may arise from siloxane RO decomposition and from ROOH rearrangement in the presence of
89 acids and H₂O. Alton and Browne (2022) predicted HCHO as a product of RO₂ rearrangement in the case of D₃ siloxane.
90 Because HCHO is a secondary product, the O₃ formation potential of D₅ may differ between source and downwind locations.

91
92 Formic acid (HCOOH) is a common acid catalyst in the atmosphere (Hazra et al., 2014) and a particle-nucleating species (Yu,
93 2000). Studies have identified some HCOOH sources in the atmosphere (Millet et al., 2015; Franco et al., 2021), however,
94 HCOOH is suspected to have unidentified anthropogenic sources in the troposphere (Millet et al., 2015; Chen et al., 2021) as
95 some urban sources remain unaccounted for (le Breton et al., 2012; Yuan et al., 2015). Chandramouli and Kamens (2001)
96 proposed that the RO₂ initially formed from D₅ + OH makes a siloxanyl formate (D₄T-OCHO, where “T” refers to CH₃SiO)
97 that reacts with H₂O to a siloxanol (D₄T-OH) and HCOOH. However, we are unaware of experimental HCOOH yields reported
98 for D₅ + OH.

99
100 Whelan et al. (2004) used known siloxane chemistry in a partitioning model to assess the atmospheric fate of siloxanes and
101 found that silanols are the predominant oxidation products. These silanols are generally water soluble and either removed from
102 the atmosphere via wet deposition, or undergo a pH-dependent process of hydrolysis, forming smaller and smaller silanols
103 (Whelan et al., 2004). Eventually, the small silanols are converted to SiO₂, H₂O, and CO₂ through photolytic reactions in water
104 or biological processes in soil (Spivack et al., 1997; Stevens, 1998; Graiver et al., 2003).

105
106 The intermediate products between D₅ and those small silanols are less well studied. The intermediates may be composed of
107 a variety of alcohols, aldehydes, and hydroperoxides if the reaction mechanisms of D₅ behave in a similar manner to that of
108 organics, with oligomers in the condensed phase (Chen et al., 2023). However, there is evidence that siloxanes do not
109 necessarily follow such reaction mechanisms (Sommerlade et al., 1993; Alton and Browne, 2020, 2022), so there is a need to
110 understand the formation of volatile oxidation products (VOP) and secondary aerosol.

111
112 Secondary aerosol mass yield (*Y*, Eq. 1) is defined as the ratio of produced aerosol mass ($\Delta m(\text{SOSiA})$) to reacted precursor
113 mass ($\Delta m(\text{D}_5)$), which we adopt here for secondary organosiloxane aerosol (SOSiA). Reports about secondary aerosol
114 formation from D₅ siloxane are conflicting, with some experiments reporting much higher *Y*_{SOSiA} than others. For instance, Wu
115 and Johnston (2017) and Janecek et al. (2019) saw maximum *Y*_{SOSiA} of 23 % and 50 %, respectively, in their photo-oxidation
116 chamber and oxidation flow reactor (OFR) experiments, albeit at different OH exposures (OH_{exp}). Charan et al. (2022) found
117 a *Y*_{SOSiA} of 158 % with their OFR at an OH_{exp} of $3.2 \times 10^{12} \text{ s cm}^{-3}$. Avery et al. (2023) reported a wide range of *Y*_{SOSiA} (2 – 146
118 %) from their PAM-OFR experiments.

119



120
$$Y_{\text{SOSiA}} = \frac{\Delta m(\text{SOSiA})}{\Delta m(\text{D}_5)} \quad (1)$$

121

122 In contrast, Charan et al. (2022) reported almost negligible Y_{SOSiA} ($< 5\%$) from their chamber studies where $[\text{OH}]$ was on the
123 order of $\sim 10^6 \text{ cm}^{-3}$, which is closer to $[\text{OH}]$ found in ambient conditions (Peng and Jimenez, 2020). Han et al. (2022) conducted
124 OFR experiments and found that Y_{SOSiA} would be 2% at $[\text{OH}]$ of $4.6 \times 10^8 \text{ cm}^{-3}$ or OH_{exp} of $5.5 \times 10^{10} \text{ s cm}^{-3}$. The variation of
125 Y_{SOSiA} reported in the literature suggests that oxidation conditions need to be considered to accurately parameterize Y_{SOSiA} ,
126 especially given that D_5 is being considered in air quality models as a part of volatile chemical product inventories (Pennington
127 et al., 2021; Seltzer et al., 2021a, b). In this study, we aim to develop parameterizations that reconcile the reported Y_{SOSiA} for
128 use in such air quality models.

129 2 Method and Materials

130 2.1 Experiments

131 The Aerodyne Research (Billerica, MA, USA) PAM-OFR (Kang et al., 2007) has a volume of 13.3 L and is made of chromated
132 aluminum (Xu and Collins, 2021). We operated the PAM-OFR in “OFR185” mode (Peng and Jimenez, 2020), where 185 nm
133 lamps that also emit 254 nm light (GPH436T5VH, LightSources, Orange, CT, USA) generate OH and O_3 with injected H_2O
134 vapor from a Nafion humidifier (FC-100-80-6MKK, Perma Pure, Lakewood, NJ, USA). There were two of these 185 nm
135 lamps placed across from each other in clear fused quartz sleeves. The 185 nm lamps were wrapped with covers at even
136 intervals to reduce the UV intensity so that 90 % of the lamp surface was covered. We operated the PAM-OFR at residence
137 times (τ_{res}) of 120 and 180 s with flow rates of 6.65 and 4.43 L min^{-1} , respectively. Additional details about the experiment
138 setup are summarized in Fig. S1 and Sect. S1.

139

140 We used the D_5 siloxane trace measured from the proton transfer reaction mass spectrometer (PTR-MS) to calculate OH_{exp}
141 with Eq. (2), where $k_{\text{D}_5+\text{OH}} = 2.0 \times 10^{-12} \text{ cm}^3 \text{ s}^{-1}$. $[\text{D}_5]_0$ and $[\text{D}_5]_{\text{final}}$ are the D_5 concentrations before and after the exposure to
142 OH.

143

144
$$\text{OH}_{\text{exp}} = -\frac{1}{k_{\text{D}_5+\text{OH}}} \times \ln\left(\frac{[\text{D}_5]_{\text{final}}}{[\text{D}_5]_0}\right) \quad (2)$$

145

146 Prior to experiments, we checked the background particle and D_5 concentrations with the scanning mobility particle sizer
147 (SMPS) and PTR-MS. In all experiments, the background particle number concentrations were $< 10 \text{ cm}^{-3}$, and the background
148 $[\text{D}_5]$ were below the limit of detection ($3\sigma = 80 \text{ ppt}$). Then, we injected D_5 with a syringe pump while monitoring the PTR-
149 MS, with major ions at m/z 371 and m/z 355. We performed the experiments with target $[\text{D}_5]_0$ of 50, 100, or 200 ppb. With
150 these target $[\text{D}_5]_0$, we get external OH reactivities (OHR_{ext}) of $2.5 - 9.8 \text{ s}^{-1}$ at 298 K and 1 atm (Peng and Jimenez, 2020).



151

152 When the D_5 trace stabilized near the target $[D_5]_0$, we began the experiment by turning on the UV lamps in the PAM-OFR to
153 either 2.4 or 8.0 V. We waited 30 minutes for the UV lamps to stabilize and for the PAM-OFR walls to equilibrate with gaseous
154 species. The Y_{SOSiA} (Eq. (1)) were calculated using the average SOSiA mass concentration from four SMPS cycles following
155 those 30 minutes. We obtained $\Delta m(D_5)$ as the difference between $[D_5]_0$ and $[D_5]_{\text{final}}$. At the end of an experiment, we turned
156 off the UV lamps to check the D_5 trace return.

157

158 To clean the PAM-OFR between experiments, we stopped the syringe pump and removed the syringe from the glass bulb
159 while keeping the humid air flow through into the PAM-OFR. We turned on the PAM-OFR UV lamps and connected the
160 outlet directly to the exhaust, until D_5 and particle number concentrations were below the limit of detection. We used Igor Pro 9
161 (Wavemetrics, Portland, OR, USA) for data post-processing and visualization.

162 2.2 Instrumentation

163 2.2.1 PTR-MS

164 To measure D_5 and VOP, we used a PTR-MS (PTR-TOF 1000, Ionicon Analytik, Innsbruck, Austria) equipped with the
165 extended volatility range (EVR) option (Piel et al., 2021), where the wetted inlet components and the drift tube are passivated
166 with a silicon coating. The PTR-MS also had an ion transfer lens between the drift tube and time-of-flight mass spectrometer
167 (Jordan et al., 2009). An internal permeation source (PerMaSCal) emitted a steady stream of 1,3-diodobenzene into the mass
168 spectrometer for mass calibration scale adjustments. Additional PTR-MS details are in Sect. S1.

169

170 To reduce H_2O clusters at high humidities, we operated the PTR-MS at 137 Td ($U_{\text{drift}} = 600$ V, Td = Townsend, 1 Td = 10^{-17}
171 V cm²) for quantification. The drift tube pressure and temperatures were set to 2.30 mbar and 80 °C. For the reagent ion source,
172 we set the U_s , U_{so} , and the H_2O flow rate to 150 V, 80 V, and 6.00 sccm respectively. The ion source hollow cathode discharge
173 current was set to 5.0 mA. The PTR-MS drift tube was 9.6 cm long, and at 137 Td, the $(H_2O)H^+$ reaction time (Δt) was 94 μs
174 (de Gouw et al., 2003). We calculated the primary reagent ion signal, $(H_2O)H^+$, by multiplying the signal of its isotope,
175 $(H_2^{18}O)H^+$, by 500.

176

177 We used the PTR-MS data for the quantification of D_5 (m/z 371), HCHO (m/z 31), and HCOOH (m/z 47), where the primary
178 reagent ion counts were normalized to 10^6 counts per second (ncps). For D_5 , we used a calibration gas cylinder (Apel-Riemer
179 Environmental, Miami, FL, USA) containing D_5 to calibrate the PTR-MS. We also calculated the normalized measurement
180 sensitivity (ncps ppb⁻¹) of D_5 , HCHO, and HCOOH using Eq. (3) adapted from de Gouw and Warneke (2007). $I_{(\text{VOC})H^+}$ and
181 $I_{(H_2O)H^+}$ are the ion counts of the protonated VOC and the reagent ion respectively. Additional details on the mass spectra
182 interpretation and quantification are in Sect. S1.5 and S3.



183

184

185

186 We tested the instrument sensitivity response with humidity by keeping the species concentrations constant while changing
187 the sample air humidity. The sensitivity of D_5 at m/z 371 was not heavily affected by humidity at 137 Td, and we did not
188 correct for humidity in the D_5 quantification (Fig. S5). On the other hand, HCHO and HCOOH sensitivities varied with
189 humidity, and we corrected their sensitivities as detailed in Sect. S3. Prior to experiments, we tuned the micro channel plate
190 (MCP) to prevent signal bias against higher mass ions (Müller et al., 2014). We adjusted the MCP voltage in steps to increase
191 the signal strength at m/z 331, a PerMaSCal ion, until the relative signal increase was $< 20\%$.

192 2.2.2 Scanning Mobility Particle Sizer

193 An SMPS (Model 3938, TSI, Shoreview, MN, USA) equipped with an impactor (0.0508 cm) measured the particle mobility
194 diameter size distribution between diameters of 14.3 to 723.4 nm. The SMPS consisted of a Model 3082 Electrostatic
195 Classifier, a Model 3081A Differential Mobility Analyzer (DMA), a Model 3088 Soft X-ray Neutralizer, and a Model 3756
196 Ultrafine Condensation Particle Counter. We set the SMPS sheath flow at 3.0 L min^{-1} and the aerosol flow rate at 0.3 L min^{-1} ,
197 and the DMA voltage ranged from 10.6 to 9921.4 V. The SMPS scanned for 150 s, followed by a 5 s retrace and 10 s purge
198 while recording on a 3 min cycle. We referred to the manufacturer's recommendations when deciding the above SMPS settings
199 (TSI Inc., 2012), and a sample particle size distribution from experiment 12 (Table 1) is shown in Fig. S4.

200

201 For the Y_{SOSiA} calculations, we converted the SMPS integrated particle volumes into mass using a SOSiA mass density (ρ_{SOSiA})
202 of 1.07 g cm^{-3} for all experiments. We obtained this ρ_{SOSiA} from PAM-OFRR experiments separate from the ones described here,
203 where we weighed the masses of SOSiA collected on filters and particle volumes with the SMPS. Additional details on ρ_{SOSiA}
204 are available in Sect. S2.

205 2.3 Volatility Distribution Parameterization

206 Janecek et al. (2019) and Charan et al. (2022) fitted their Y_{SOSiA} data to the Odum two-product model (Odum et al., 1996) and
207 we follow the same methodology for comparison with the literature (Sect. S4). Similarly, we fit the standard volatility basis
208 set (VBS) parameters α (Donahue et al., 2006) in Eq. (4) to the measured $\Delta m(\text{SOSiA})$ using the measured $\Delta m(D_5)$, where α_i is
209 the product mass yield for volatility bin i .

210

211

212

$$\Delta m(\text{SOSiA}) = \Delta m(D_5) \times \sum_{i=1}^n \frac{\alpha_i}{1 + \frac{c_i^*}{c_{\text{OA}}^*}} \quad (4)$$

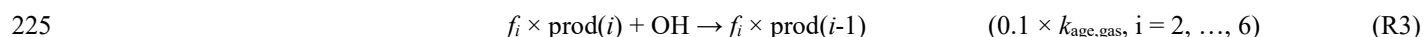
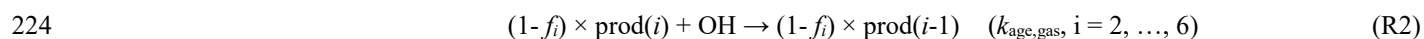
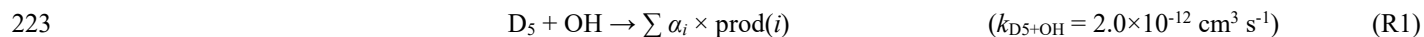


213 In the experiments, the organosiloxane aerosol mass loading (C_{OA}) was equivalent to the SOSiA mass concentrations. As the
 214 produced aerosol mass in the experiments ranged from 3.7 to $\sim 1000 \mu\text{g m}^{-3}$, we use six logarithmically spaced effective
 215 saturation mass concentration (C^*) bins ranging from 0.1 to $10000 \mu\text{g m}^{-3}$ at 298 K to cover the low and high-volatility products.
 216 For reference, D_5 liquid has a vapor pressure of 20.4 Pa at 298 K or $C^* = 3.05 \times 10^6 \mu\text{g m}^{-3}$ (Lei et al., 2010).

217

218 As the experiments were performed for a range of OH_{exp} , the products between experiments may have varied due to
 219 multigenerational aging (Zhao et al., 2015). To account for aging and parameterize Y_{SOSiA} as a function of OH exposure, we
 220 also analyse the yield data using a kinetic box model with four chemical reactions (R1–R3) written in MATLAB (MathWorks,
 221 Natick, MA, USA).

222



226

227 Eq. (R1) describes the initial oxidation of D_5 and formation of RO_2 , which immediately forms products of varying volatility
 228 (Eq. (R2)). Here, $\text{prod}(i)$ refers to the sum of products (gas + particle) in volatility bin i , which are formed with a molar
 229 branching ratio α_i . We assume that $\text{prod}(i)$ have the same molecular weights (g mol^{-1}) as D_5 , and so the α_i are equivalent to the
 230 product mass yields at $\text{OH}_{\text{exp}} \rightarrow 0$. In the model, a fraction f_i of each oxidation product partitions instantaneously from the gas
 231 phase to the particle phase according to absorptive partitioning theory (Donahue et al., 2006) (Eq. 5).

232

$$233 \quad f_i = \left(\frac{1}{1 + \frac{c_i^*}{c_{OA}}} \right) \quad (5)$$

234

235 Eqs. (R2) and (R3) describe how OH_{exp} causes volatility to decrease (Robinson et al., 2007). This decrease in volatility via
 236 “bin-hopping” (Sommers et al., 2022) occurs at a rate proportional to the chemical aging rate coefficient for gaseous species
 237 ($k_{\text{age,gas}}, \text{cm}^3 \text{ s}^{-1}$), with the oxidation of particle-phase products being ten times slower than that of the gas. Note that we assume
 238 that products in the lowest-volatility bin cannot be removed from that bin and that the highest-volatility bin does not receive
 239 product with aging ($i = 2, \dots, 6$). The $[\text{OH}]$ are set by dividing the experimental OH_{exp} from Eq. 2 by the PAM-OFr residence
 240 times.

241

242 We use $k_{\text{age,gas}}$ and $k_{\text{age,particle}}$ as aggregate chemical aging rate coefficients, not specific to any species or volatility bin. Studies
 243 on chamber experiments (Robinson et al., 2007) and ambient measurements (Sommers et al., 2022) applied chemical aging
 244 only to the gas phase as heterogeneous aging is relatively slower. However, studies have found that the high oxidant



245 concentrations in OFRs would appreciably oxidize OA within experiment timescales (Kessler et al., 2012; Kroll et al., 2015).
246 To accommodate OH uptake to the bulk phase, we follow the approach used by Zhao et al. (2015) and assume that the effective
247 particle-phase aging rate coefficient ($k_{\text{age,particle}}$) is equivalent to 10 % of the gas-phase aging rate coefficient ($k_{\text{age,gas}}$). The
248 timescales and atmospheric relevance of heterogeneous oxidation in OFRs are areas of ongoing research (Zhao et al., 2019;
249 Peng and Jimenez, 2020), but for now we opt to fit a single chemical aging rate coefficient to reduce dimensionality. We use
250 the Monte Carlo genetic algorithm (Berkemeier et al., 2017) to fit $k_{\text{age,gas}}$ and the six coefficients α_i .

251 3 Results and Discussion

252 3.1 Volatile Organic Products (VOP)

253 3.1.1 Siloxanol and Formate Ester Trends

254 Fig. 1 shows the PTR-MS mass spectra for experiment 12 (Table 1), where $[D_5]_0$ and OH_{exp} were high. The PTR-MS signals
255 before and after D_5 is oxidized are displayed relative to the protonated D_5 ion at m/z 371 to identify changes more easily in the
256 mass spectra. Using the mass spectra and species reported by Alton and Browne (2022), we attribute the indicated ions in Fig.
257 1 to siloxanol ($D_4T\text{-OH}$), siloxanediol ($D_3T_2\text{-(OH)}_2$), siloxanyl formate ($D_4T\text{-OCHO}$), and siloxanolyl formate ($D_3T_2\text{-OH-}$
258 OCHO). Here, “D” and “T” refers to units of $(\text{CH}_3)_2\text{SiO}$ and CH_3SiO respectively. The multifunctional VOP are reported to
259 arise from multiple steps of oxidation (Alton and Browne, 2022).

260

261 D_5 siloxane loses a methyl group during the PTR, which forms a large signal at m/z 355. The isotopologues of the $-\text{CH}_3$
262 fragment of D_5 overlap with fragments of VOP, which complicates the VOP identification. To separate the signal of the VOP,
263 we use the ratios of the D_5 signal and its $-\text{CH}_3$ signals prior to oxidation. The red and pink shaded areas in the inset of Fig. 1
264 refer to the enhancement in signal over that of the $-\text{CH}_3$ fragment of D_5 , which we attribute to the $-\text{OH}$ fragments of $D_4T\text{-OH}$
265 and $D_3T_2\text{-(OH)}_2$, respectively. We use the masses of the $-\text{OH}$ fragments of the siloxanols as large alcohols dissociate during
266 the PTR (Brown et al., 2010).

267

268 As we did not have calibration standards to quantify these VOP, we calculate the relative molar yields of the VOP to that of
269 protonated D_5 siloxane at m/z 371 to study the trends of siloxane VOP (Fig. 2). The y-axes in Fig. 2 are the relative molar
270 yields (ncps/ncps), which refers to the change in signal attributed to a VOP over that of m/z 371. Δm_{371} refers to the change
271 in the signal at m/z 371 before and after OH oxidation. In the right-side panels for each VOP in Fig. 2, the relative molar yield
272 of VOP decreases with increasing OH_{exp} (x-axes). This decrease in VOP signal is consistent with these gaseous products
273 undergoing further oxidation or increased gas-particle partitioning due to higher C_{OA} at higher OH_{exp} .

274



275 In the left-side panels for each VOP in Fig. 2, the relative signals of the VOP (y-axes) decreases with increasing OH_{exp} (color
276 scale). Then, assuming $[\text{OH}]$ is consistent throughout the PAM-OFR, that $\text{D}_5 + \text{OH}$ is the rate-limiting step in VOP formation,
277 and that removal via gas-particle partitioning is negligible, we can consider a simplified $\text{D}_5 + \text{OH}$ chemical mechanism, (R4)
278 and (R5).

279



282

283 In Eq. (R4), γ_i is the relative molar yield of a given VOP_i found by extrapolating $\Delta m(\text{VOP}_i)/\Delta m_{371}$ (y-axes in Fig. 2) to OH_{exp}
284 $\rightarrow 0$. With ordinary differential equations (ODE) from these reactions (Eq. (7) and (8)) and experimental inputs, we fit γ_i and
285 the $\text{VOP}_i + \text{OH}$ rate coefficient ($k_{\text{VOP}_i+\text{OH}}$, $\text{cm}^3 \text{ s}^{-1}$). The fits are shown as black lines in the right-side panels of each VOP in
286 Fig. 2.

287

$$288 \quad \frac{d[\text{D}_5]}{dt} = -k_{\text{D}_5+\text{OH}}[\text{D}_5][\text{OH}] \quad (7)$$

289

$$290 \quad \frac{d[\text{VOP}_i]}{dt} = \gamma_i k_{\text{D}_5+\text{OH}}[\text{D}_5][\text{OH}] - k_{\text{VOP}_i+\text{OH}}[\text{VOP}_i][\text{OH}] \quad (8)$$

291

292 The fitted $k_{\text{VOP}_i+\text{OH}}$ for each VOP are on the order of $\sim 10^{-12} \text{ cm}^3 \text{ s}^{-1}$ (Table S7), but faster than $k_{\text{D}_5+\text{OH}}$, which suggests that these
293 VOP have atmospheric lifetimes shorter than that of D_5 . Alton and Browne (2022) have estimated these VOP to be volatile
294 with quantitative structure activity relationship models. However, there are uncertainties in those models, and the VOP may
295 have lower saturation mass concentrations than expected. Moreover, the chemical mechanism might be more complex than
296 the one outlined with the simple reactions (R4) and (R5). Consequently, we present these $k_{\text{VOP}_i+\text{OH}}$ as estimates for secondary
297 chemistry in this simplified reaction scheme, and future work using quantitative measurements should improve the calculated
298 lifetimes of these intermediate $\text{D}_5 + \text{OH}$ products in the atmosphere.

299 3.1.2 Formaldehyde (HCHO) Yields

300 As shown in Table S8 and Fig. 3, the experimental molar yields of HCHO (Y_{HCHO} , $\Delta \text{HCHO}/\Delta \text{D}_5$ in ppb/ppb) exceed 100 % at
301 low OH_{exp} and decrease with higher OH_{exp} . We attribute the decreasing Y_{HCHO} with increasing OH_{exp} to HCHO removal by OH
302 in the PAM-OFR. HCHO has a lifetime of 0.91 days at $[\text{OH}]_{\text{avg}} = 1.5 \times 10^6 \text{ cm}^{-3}$ (Atkinson et al., 2006) or 78 s at $[\text{OH}] = 1.5$
303 $\times 10^9 \text{ cm}^{-3}$. In such high $[\text{OH}]$ conditions, some HCHO is oxidized while being produced, which is consistent with the
304 decreasing Y_{HCHO} with increasing OH_{exp} (Fig. 3a1). Thus, we use the ODE from Eqs. (7) and (8) and a fixed $k_{\text{HCHO}+\text{OH}} = 8.5 \times$
305 $10^{-12} \text{ cm}^3 \text{ s}^{-1}$ at 298 K to obtain the molar yield of HCHO as $\text{OH}_{\text{exp}} \rightarrow 0$, which we denote as γ_{HCHO} .

306



307 We fit γ_{HCHO} to be 269 % (black line in Fig. 3a2), assuming a constant [OH] in the PAM-OFR, that HCHO is rapidly formed
308 from $\text{D}_5 + \text{OH}$, and that HCHO removal via partitioning or reactive uptake is negligible. This γ_{HCHO} is consistent with the
309 modeled yields of those for VOC used by Millet et al. (2006), who used γ_{HCHO} from chemical models ranging from 60 – 230
310 % for a variety of VOC. Thus, D_5 has a comparable γ_{HCHO} to that of isoprene or aromatic VOC.

311

312 Fu et al. (2020) proposed a mechanism for D_3 siloxane, where high Y_{HCHO} is produced under low NO/HO_2 conditions. In that
313 mechanism, RO_2 rearrangement and RO H-shift rate coefficients become progressively faster as the D_3 siloxane backbone is
314 oxidized, and HCHO is produced at each rearrangement step. The γ_{HCHO} exceeding 100 % in these D_5 experiments is consistent
315 with HCHO production over multiple rapid oxidation steps. The results we report suggests that a similar HCHO production
316 mechanism exists for D_5 .

317

318 Mao et al. (2009) found that models under-predicted tropospheric HCHO during their aircraft campaign studying Asian
319 pollution outflows into the Pacific ocean. This discrepancy between the measurements and calculations was pronounced near
320 the surface and up to 2 km. They proposed that there is some missing OH reactivity, and that the unaccounted species would
321 be reactive with OH and yield HCHO when oxidized. Based on the D_5 experiments present here, the inclusion of siloxane
322 species may reduce the HCHO formation gap; Coggon et al. (2021) already noted that including volatile chemical products in
323 their model would increase HCHO production.

324

325 The large formation of HCHO may entail that D_5 siloxane could contribute to O_3 formation, albeit indirectly. We were unable
326 to observe O_3 enhancement due to the high concentrations of O_3 produced from the PAM-OFR internal chemistry itself and
327 the lack of NO_x . Given that $k_{\text{D}_5+\text{OH}}$ is relatively slow compared to that of other common anthropogenic VOC, we suspect that
328 the oxidation of D_5 will occur downwind of urban sources in low- NO_x conditions or in cases of air stagnation. Whether D_5 has
329 a net positive or negative effect on O_3 formation in these VOC/ NO_x scenarios needs to be assessed with models. To get a rough
330 estimate of O_3 production, we consider a case where 20 ppt of D_5 react with OH to form 40 ppt of HCHO, which also fully
331 react. This D_5 concentration is within the range reported by Coggon et al. (2018) in ambient urban air. The molar maximum
332 incremental reactivity (MIR) of HCHO under high- NO_x conditions is ~20 % (Carter et al., 1995), which makes HCHO a
333 prominent precursor for tropospheric O_3 . By multiplying the MIR with the HCHO reacted with OH, we can estimate an O_3
334 formation potential of 8 ppt from D_5 in urban air.

335 3.1.3 Formic Acid (HCOOH) Yields

336 We find molar yields of HCOOH (Y_{HCOOH} , $\Delta\text{HCOOH}/\Delta\text{D}_5$ ppb/ppb) between 45 – 127 %, as shown in Fig. 3b, although a
337 trend with OH_{exp} is not obvious (Fig. 3b). We assume HCOOH loss via OH oxidation to be minor given the rate coefficient of
338 $k_{\text{HCOOH}+\text{OH}} = 4.5 \times 10^{-13} \text{ cm}^3 \text{ s}^{-1}$ at 298 K (Atkinson et al., 2006), which corresponds to 17 days of OH_{exp} at $[\text{OH}]_{\text{avg}} = 1.5 \times 10^6$
339 cm^{-3} or an OH-oxidation lifetime of 440 s in our highest OH_{exp} experiment. In addition to $\text{D}_4\text{T-OCHO}$ hydrolysis, HCOOH



340 may have been produced by heterogeneous reactions of HCHO at the surface of the SOSiA or the OFR walls in these humid
341 experiments. In the atmosphere, HCOOH is presumed to form heterogeneously from HCHO and methanediol (HOCH₂OH) in
342 the presence of wet particles (Franco et al., 2021).

343

344 The Y_{HCOOH} from D₅ + OH we report are higher than the values from isoprene + OH (Link et al., 2020) or monoterpene + OH
345 reported by Friedman and Farmer (2018), who quantified the Y_{HCOOH} of 7 monoterpenes at varying OH_{exp} without NO_x. The
346 range of Y_{HCOOH} from these references is shown as shaded areas in Fig. 3b2. The Y_{HCOOH} from D₅ is on par with the humid
347 isoprene ozonolysis cases reported by Link et al. (2020). Friedman and Farmer (2018) also used a PAM-OFR, but with 254
348 nm UV lamps in dry conditions (~1 % RH), and Link et al. (2020) used a reaction chamber, which limits a direct comparison
349 with our results. Nevertheless, Friedman and Farmer (2018) found Y_{HCOOH} of 0.64 – 8.5 % at $\text{OH}_{\text{exp}} = 2.0 \times 10^{11} \text{ s cm}^{-3}$. Aside
350 from the different precursor VOC and mechanism, Friedman and Farmer (2018) may have encountered less heterogenous
351 production of HCOOH due to the dry OFR conditions. Our laboratory findings suggest that D₅ siloxane should be considered
352 as an atmospheric HCOOH source.

353 3.2 SOSiA Mass Yields

354 3.2.1 Volatility Basis Set Parameterization

355 The Odum two-product model does not reconcile the Y_{SOSiA} in the literature in the high C_{OA} range (Sect. S4), so we apply a
356 VBS model. Fig. 4a shows the fitted aerosol mass yield curve (black line) using a standard-VBS model (Eq. (4)), but the Y_{SOSiA}
357 (y-axis) appears to depend on both C_{OA} (x-axis) and OH_{exp} (color scale). To address whether accounting for the varying OH_{exp}
358 in these experiments would improve the VBS model outputs, we fit the produced SOSiA mass using a standard-VBS model
359 (Eq. (4)) and a kinetic model with VBS and chemical aging rate coefficients (“aging-VBS model”, Eqs. (R1) – (R3)) based on
360 OH_{exp} and $[\text{D5}]_0$ (Table 1). We fit $k_{\text{age,gas}}$ in Eq. (R2) to be $2.17 \times 10^{-11} \text{ cm}^3 \text{ s}^{-1}$. The fitted VBS parameters are summarized in
361 Table S11.

362

363 In both the standard and aging-VBS model fits (blue and red, respectively in Fig. 4b), ~95 % of the D₅ + OH product mass is
364 in the gas phase at a C_{OA} of $10 \mu\text{g m}^{-3}$. The high fraction of gaseous products is consistent with low Y_{SOSiA} in the lower OH_{exp}
365 experiments, whereas additional oxidation in the higher OH_{exp} experiments leads to a shift towards products that partition into
366 the particle phase, thus increasing Y_{SOSiA} . Secondary organic aerosol (SOA) often exhibits a maximum yield as a function of
367 OH_{exp} , after which the yield decreases due to fragmentation becoming dominant at high OH_{exp} (Isaacman-VanWertz et al.,
368 2018). We do not find such a maximum in the range of OH_{exp} studied, which suggests that an even higher Y_{SOSiA} could have
369 been found at higher OH_{exp} . Moreover, SOSiA is reported to be non-hygroscopic compared to SOA (Janecek et al., 2019),
370 and we do not see an obvious relationship between the experiment humidity conditions and aerosol formation.

371



372 Figs. 4c and 4d show comparisons of the standard and aging-VBS with experimental SOSiA mass concentrations and Y_{SOSiA} .
373 We see an improvement in the R^2 with the aging-VBS over the standard-VBS model, suggesting that incorporating OH_{exp} into
374 the yield parameterization improves model outcomes. Fig. 5 illustrates compares the standard-VBS model with the aging VBS
375 for a range of OH_{exp} , showing that product volatility gradually decreases with increasing OH_{exp} in the ageing VBS model. The
376 high volatility of the initial products is consistent with the lack of the rapid formation of low-volatile species, like highly
377 oxygenated molecules, known to form SOA (Isaacman-VanWertz et al., 2018).

378 3.2.2 Reconciling Literature Y_{SOSiA}

379 To address the variation in the literature Y_{SOSiA} and to generate parameters for air quality models, we fit the parameters in the
380 aging-VBS model with all available data in the literature and those from our experiments. Given that the literature used
381 differing ρ_{SOSiA} to calculate Y_{SOSiA} from SMPS data, we adjust the Y_{SOSiA} and C_{OA} reported in the literature to that of the ρ_{SOSiA}
382 used here ($\rho_{\text{SOSiA}} = 1.07 \text{ g cm}^{-3}$). Similarly, we re-calculate the OH_{exp} in the literature using Eq. (2) and the $[\text{D}_5]_0$ and $[\text{D}_5]_{\text{final}}$
383 values.

384

385 Fig. 6 shows experimental values (markers) and model outputs (contours) of Y_{SOSiA} (panels a1 and a2) and SOSiA mass
386 concentrations (panels b1 and b2) as a function of $[\text{D}_5]_0$ and OH_{exp} . Figs. 6a1 and 6b1 are generated using the aging-VBS
387 model fit using only data from experiments presented in this study, while Figs. 6a2 and 6b2 show a fit including data from the
388 literature. The aging-VBS model is able to capture the increasing Y_{SOSiA} with increasing $[\text{D}_5]_0$ and OH_{exp} . At a given $[\text{D}_5]_0$,
389 Y_{SOSiA} and the SOSiA mass concentration increase with higher OH_{exp} . Fig. 6a2 shows that the relatively high Y_{SOSiA} ($> 50\%$)
390 is feasible at $\text{OH}_{\text{exp}} > 10^{12} \text{ s cm}^3$. Moreover, the aging-VBS model predicts that Y_{SOSiA} is almost negligible ($< 5\%$) under
391 atmospheric concentrations of D_5 and OH_{exp} .

392

393 Fig. S8 shows that the aging-VBS model used here leads to a much higher correlation between modelled and experimental
394 values for SOSiA mass concentration compared to the same analysis with a standard-VBS model ($R^2 = 0.956$ vs. $R^2 = 0.745$).
395 The better correlation suggests that the volatility distribution evolves with OH_{exp} and that chemical aging should be considered
396 when evaluating the volatility distribution of SOSiA from $\text{D}_5 + \text{OH}$.

397

398 We note that, in reality, bulk-phase chemistry is more complex than logarithmic shifts in volatility with OH_{exp} and not fully
399 captured in the above aging-VBS parameterization. For example, Wu and Johnston (2017), Avery et al. (2023), and Chen et
400 al. (2023) characterized $\text{D}_5 + \text{OH}$ SOSiA with mass spectrometry and found spectra indicative of oligomers. The formation of
401 oligomers may reduce the bulk volatility by more than one bin and change the gas-particle equilibrium timescales (Berkemeier
402 et al., 2020). Here, we incorporated $k_{\text{age,gas}}$ and a simple “bin-hopping” approach to illustrate that a change in the volatility
403 distribution with OH_{exp} can adequately reconcile the Y_{SOSiA} variation in the literature. Future work with more sophisticated
404 chemical models should close that gap further.



405 4 Conclusions and Atmospheric Implications

406 With a PAM-OFR, PTR-MS, and SMPS, we studied the formation of VOP and SOSiA under various OH_{exp} conditions. Using
407 a simplified VOP oxidation scheme (Eqs. (R5) and (R6)), we find that the VOP of tentatively identified siloxanols and formate
408 esters have shorter OH-oxidation lifetimes than their precursor D₅ (Table S7). In addition, we find the mass yield of HCHO of
409 D₅ comparable to that of isoprene or aromatics (Millet et al., 2006), suggesting that D₅ siloxane is a potential O₃-contributing
410 species in downwind scenarios. We find the mass yield of HCOOH ranging from 45 – 127 %, which suggests that D₅ + OH is
411 a source of atmospheric HCOOH.

412

413 An aging-VBS model incorporating OH_{exp} and chemical aging adequately describes gas-particle partitioning at atmospheric
414 OH_{exp} and C_{OA}. Based on these experiments, low-NO_x Y_{SOSiA} should be < 10 % under commonly observed atmospheric OH_{exp}
415 < 5 × 10¹¹ s cm⁻³ (Fig. 6a1). The first-generation products of D₅ + OH are likely volatile, but their volatility decreases with
416 increasing OH_{exp} (Fig. 5). This shift in volatility suggests that further oxidation of secondary products would reduce the
417 volatility enough to form SOSiA. Unlike α-pinene (Isaacman-VanWertz et al., 2018) or other precursors for secondary organic
418 aerosol (SOA), D₅ + OH does not appear to produce low-volatile species within a single oxidation step. Instead, additional
419 OH_{exp} is needed to form aerosol, which suggests that multiple oxidation steps lead to gradual decrease of product volatility.
420 Hence, concepts that can be successfully applied to SOA formation may not accurately capture SOSiA formation, for which
421 models must consider chemical aging. In the atmosphere, SOSiA from D₅ + OH may be easier to detect downwind of urban
422 sources due to the higher OH_{exp} and dilution/removal of competing OH-reactive species.

423

424 Based on KinSim calculations (Sect. S5), we expect that the RO₂ fate is dominated by RO₂ + HO₂ and RO₂ + OH, which is
425 consistent with the calculations performed by Avery et al. (2023). However, we note that the reaction rate coefficients of RO₂
426 and its subsequent products are uncertain for D₅, and we cannot directly address the atmospheric relevance of these calculated
427 RO₂ fates at this time. To improve Y_{SOSiA} parameterizations for the atmosphere, there is a need to study the impact NO_x has on
428 siloxane RO₂ chemistry, given that siloxanes are likely emitted from urban sources where [NO_x] is high. In such scenarios,
429 RO₂ + NO_x is likely an important fate (Peng et al., 2019; Newland et al., 2021). Han et al. (2022) found that the addition of
430 N₂O into their OFR would reduce Y_{SOSiA}, although the cause is unclear. However, Charan et al. (2022) did not find Y_{SOSiA} to
431 change with NO_x in their chamber experiments, which is consistent with rapid RO formation across RO₂ fates. Quantifying
432 secondary species across RO₂ fates and identifying their subsequent oxidation reactions may also be useful to adapt the D₅
433 oxidation mechanism into chemical kinetics models.

434

435 The high [OH] used in OFRs may induce faster radical reactions and dimerization near the particle surface (Zhao et al., 2019),
436 which affects particle composition and equilibrium timescales. Dimers and oligomers have been found in SOSiA (Wu and
437 Johnston, 2017; Avery et al., 2023; Chen et al., 2023), and how oligomerization in the D₅ + OH SOSiA system evolves the



438 volatility distribution and particle properties is currently not considered in the aging-VBS model. Moreover, high degrees of
439 oxidation should lead to fragmentation and increasing volatility (Isaacman-VanWertz et al., 2018), which is also not considered
440 in the aging-VBS model. Hence, multiphase modeling to evaluate SOSiA chemistry and translate experimental findings to
441 atmospheric conditions remains a direction for future research.

442 **Appendix A Abbreviations**

443 C_{OA} : organic aerosol mass loading
444 C^* : effective saturation mass concentration
445 D_5 : decamethylcyclopentasiloxane
446 EVR: extended volatility range
447 ID: inner diameter of tubing
448 I_{254} , I_{185} : flux of 254 and 185 nm photons
449 OA: organic aerosol
450 OD: outer diameter of tubing
451 OFR: oxidation flow reactor
452 OH: hydroxyl radical
453 $[OH]_{avg}$: 24 hour average daily hydroxyl radical concentration
454 OH_{exp} : hydroxyl radical exposure
455 OHR_{ext} : external hydroxyl radical reactivity
456 O_3 : ozone
457 ncps: normalized counts per second
458 NO_x : nitric oxide and nitrogen dioxide
459 PAM: potential aerosol mass
460 PTR: proton transfer reaction
461 PTR-MS: proton transfer reaction mass spectrometer
462 RH: relative humidity
463 RO: alkoxy radical
464 RO_2 : peroxy radical
465 SMPS: scanning mobility particle sizer
466 SOA: secondary organic aerosol
467 SOSiA: secondary organosiloxane aerosol
468 UV: ultraviolet radiation
469 VBS: volatility basis set



- 470 VOP: volatile oxidation products
471 Y_{HCHO} : formaldehyde molar yield from D_5
472 Y_{HCOOH} : formic acid molar yield from D_5
473 Y_{SOSiA} : SOSiA mass yield from D_5
474 γ : molar yields extrapolated to when $\text{OH}_{\text{exp}} \rightarrow 0$
475 ρ_{SOSiA} : SOSiA aerosol mass density
476 τ_{res} : residence time

477 **Data Availability**

478 Summary data are available in the supplementary. Additional data will be provided upon reasonable request.

479 **Author ORCID**

- 480 Hyun Gu Kang: <https://orcid.org/0000-0002-3320-9447>
481 Yanfang Chen: <https://orcid.org/0000-0002-4415-7398>
482 Jiwoo Jeong: <https://orcid.org/0000-0002-4038-8148>
483 Yoojin Park: <https://orcid.org/0000-0002-4832-8633>
484 Thomas Berkemeier: <https://orcid.org/0000-0001-6390-6465>
485 Hwajin Kim: <https://orcid.org/0000-0001-6138-6443>

486 **Author Contribution**

487 HGK, YC, JJ, and YP conducted the experiments. YP performed the offline calibrations of OH exposure on the PAM-OFR.
488 HGK analysed the data. HGK and TB developed the kinetic model. HGK, HK and TB wrote the manuscript with contributions
489 from all co-authors. HK supervised the project.

490 **Competing Interests**

491 TB is a member of the editorial board of Atmospheric Chemistry and Physics, but the peer-review process was guided by an
492 independent editor. The authors declare that they have no other personal nor financial conflicts of interest. Instruments and
493 products used in the research are listed for reference and not as endorsements.



494 **Acknowledgements**

495 This work was supported by the FRIEND Project (Fine Particle Research Initiative in East Asia Considering National
496 Differences), which is funded by the National Research Foundation of Korea (NRF) and the Ministry of Science and ICT of
497 the Republic of Korea (2022M3G1A1020858). Also funded by National Research Foundation of Korea (NRF) funded by the
498 Ministry of Science and ICT (NRF-2021R1A2C2004365). HGK is supported by the Max Planck Graduate Center with
499 Johannes Gutenberg University Mainz. APM Engineering (Gyeonggi-do, South Korea) rent the PTR-MS, and the authors
500 thank BO for maintaining it.

501 **References**

502 Alton, M. W. and Browne, E. C.: Atmospheric Chemistry of Volatile Methyl Siloxanes: Kinetics and Products of Oxidation
503 by OH Radicals and Cl Atoms, *Environ Sci Technol*, 54, 5992–5999, <https://doi.org/10.1021/acs.est.0c01368>, 2020.

504

505 Alton, M. W. and Browne, E. C.: Atmospheric Degradation of Cyclic Volatile Methyl Siloxanes: Radical Chemistry and
506 Oxidation Products, *ACS Environmental Au*, <https://doi.org/10.1021/acsenvironau.1c00043>, 2022.

507

508 Arata, C., Misztal, P. K., Tian, Y., Lunderberg, D. M., Kristensen, K., Novoselac, A., Vance, M. E., Farmer, D. K., Nazaroff,
509 W. W., and Goldstein, A. H.: Volatile organic compound emissions during HOMEChem, *Indoor Air*, 31, 2099–2117,
510 <https://doi.org/https://doi.org/10.1111/ina.12906>, 2021.

511

512 Atkinson, R.: Kinetics of the gas-phase reactions of a series of organosilicon compounds with hydroxyl and nitrate(NO₃)
513 radicals and ozone at 297 ± 2 K, *Environ Sci Technol*, 25, 863–866, <https://doi.org/10.1021/es00017a005>, 1991.

514

515 Atkinson, R., Baulch, D. L., Cox, R. A., Crowley, J. N., Hampson, R. F., Hynes, R. G., Jenkin, M. E., Rossi, M. J., Troe, J.,
516 and Subcommittee, I.: Evaluated kinetic and photochemical data for atmospheric chemistry: Volume II – gas phase
517 reactions of organic species, *Atmos Chem Phys*, 6, 3625–4055, <https://doi.org/10.5194/acp-6-3625-2006>, 2006.

518

519 Avery, A. M., Alton, M. W., Canagaratna, M. R., Krechmer, J. E., Sueper, D. T., Bhattacharyya, N., Hildebrandt Ruiz, L.,
520 Brune, W. H., and Lambe, A. T.: Comparison of the Yield and Chemical Composition of Secondary Organic Aerosol
521 Generated from the OH and Cl Oxidation of Decamethylcyclopentasiloxane, *ACS Earth Space Chem*,
522 <https://doi.org/10.1021/acsearthspacechem.2c00304>, 2023.

523



524 Berkemeier, T., Ammann, M., Krieger, U. K., Peter, T., Spichtinger, P., Pöschl, U., Shiraiwa, M., and Huisman, A. J.:
525 Technical note: Monte Carlo genetic algorithm (MCGA) for model analysis of multiphase chemical kinetics to determine
526 transport and reaction rate coefficients using multiple experimental data sets, *Atmos Chem Phys*, 17, 8021–8029,
527 <https://doi.org/10.5194/acp-17-8021-2017>, 2017.

528

529 Berkemeier, T., Takeuchi, M., Eris, G., and Ng, N. L.: Kinetic modeling of formation and evaporation of secondary organic
530 aerosol from NO₃ oxidation of pure and mixed monoterpenes, *Atmos Chem Phys*, 20, 15513–15535,
531 <https://doi.org/10.5194/acp-20-15513-2020>, 2020.

532

533 Le Breton, M., McGillen, M. R., Muller, J. B. A., Bacak, A., Shallcross, D. E., Xiao, P., Huey, L. G., Tanner, D., Coe, H., and
534 Percival, C. J.: Airborne observations of formic acid using a chemical ionization mass spectrometer, *Atmos. Meas. Tech.*, 5,
535 3029–3039, <https://doi.org/10.5194/amt-5-3029-2012>, 2012.

536

537 Brown, P., Watts, P., Märk, T. D., and Mayhew, C. A.: Proton transfer reaction mass spectrometry investigations on the effects
538 of reduced electric field and reagent ion internal energy on product ion branching ratios for a series of saturated alcohols, *Int*
539 *J Mass Spectrom*, 294, 103–111, <https://doi.org/https://doi.org/10.1016/j.ijms.2010.05.028>, 2010.

540

541 Carter, W. P. L., Pierce, J. A., Malkina, I. L., Luo, D., and Long, W. D.: ENVIRONMENTAL CHAMBER CHAMBER
542 STUDIES STUDIES OF OF MAXIMUM MAXIMUM INCREMENTAL INCREMENTAL REACTIVITIES
543 REACTIVITIES OF OF VOLATILE VOLATILE ORGANIC ORGANIC COMPOUNDS COMPOUNDS, 1993.

544

545 Carter, W. P. L., Pierce, J. A., Luo, D., and Malkina, I. L.: Environmental chamber study of maximum incremental reactivities
546 of volatile organic compounds, *Atmos Environ*, 29, 2499–2511, [https://doi.org/https://doi.org/10.1016/1352-2310\(95\)00149-](https://doi.org/https://doi.org/10.1016/1352-2310(95)00149-S)
547 *S*, 1995.

548

549 Chandramouli, B. and Kamens, R. M.: The photochemical formation and gas–particle partitioning of oxidation products of
550 decamethyl cyclopentasiloxane and decamethyl tetrasiloxane in the atmosphere, *Atmos Environ*, 35, 87–95,
551 [https://doi.org/https://doi.org/10.1016/S1352-2310\(00\)00289-2](https://doi.org/https://doi.org/10.1016/S1352-2310(00)00289-2), 2001.

552

553 Charan, S. M., Huang, Y., Buenconsejo, R. S., Li, Q., Cocker III, D. R., and Seinfeld, J. H.: Secondary organic aerosol
554 formation from the oxidation of decamethylcyclopentasiloxane at atmospherically relevant OH concentrations, *Atmos Chem*
555 *Phys*, 22, 917–928, <https://doi.org/10.5194/acp-22-917-2022>, 2022.

556



- 557 Chen, X., Millet, D. B., Neuman, J. A., Veres, P. R., Ray, E. A., Commane, R., Daube, B. C., McKain, K., Schwarz, J. P.,
558 Katich, J. M., Froyd, K. D., Schill, G. P., Kim, M. J., Crouse, J. D., Allen, H. M., Apel, E. C., Hornbrook, R. S., Blake, D.
559 R., Nault, B. A., Campuzano-Jost, P., Jimenez, J. L., and Dibb, J. E.: HCOOH in the Remote Atmosphere: Constraints from
560 Atmospheric Tomography (Atom) Airborne Observations, *ACS Earth Space Chem*, 5, 1436–1454,
561 <https://doi.org/10.1021/acsearthspacechem.1c00049>, 2021.
- 562
- 563 Chen, Y., Park, Y., Kang, H. G., Jeong, J., and Kim, H.: Chemical characterization and formation of secondary organosiloxane
564 aerosol (SOSiA) from OH oxidation of decamethylcyclopentasiloxane, *Environ. Sci.: Atmos.*,
565 <https://doi.org/10.1039/D2EA00161F>, 2023.
- 566
- 567 Cheng, Z., Qiu, X., Shi, X., and Zhu, T.: Identification of organosiloxanes in ambient fine particulate matters using an
568 untargeted strategy via gas chromatography and time-of-flight mass spectrometry, *Environmental Pollution*, 271, 116128,
569 <https://doi.org/https://doi.org/10.1016/j.envpol.2020.116128>, 2021.
- 570
- 571 Coggon, M. M., McDonald, B. C., Vlasenko, A., Veres, P. R., Bernard, F., Koss, A. R., Yuan, B., Gilman, J. B., Peischl, J.,
572 Aikin, K. C., DuRant, J., Warneke, C., Li, S.-M., and de Gouw, J. A.: Diurnal Variability and Emission Pattern of
573 Decamethylcyclopentasiloxane (D5) from the Application of Personal Care Products in Two North American Cities, *Environ*
574 *Sci Technol*, 52, 5610–5618, <https://doi.org/10.1021/acs.est.8b00506>, 2018.
- 575
- 576 Coggon, M. M., Gkatzelis, G. I., McDonald, B. C., Gilman, J. B., Schwantes, R. H., Abuhassan, N., Aikin, K. C., Arend, M.
577 F., Berkoff, T. A., Brown, S. S., Campos, T. L., Dickerson, R. R., Gronoff, G., Hurley, J. F., Isaacman-VanWertz, G., Koss,
578 A. R., Li, M., McKeen, S. A., Moshary, F., Peischl, J., Pospisilova, V., Ren, X., Wilson, A., Wu, Y., Trainer, M., and Warneke,
579 C.: Volatile chemical product emissions enhance ozone and modulate urban chemistry, *Proceedings of the National Academy*
580 *of Sciences*, 118, e2026653118, <https://doi.org/10.1073/pnas.2026653118>, 2021.
- 581
- 582 Derwent, R. G., Jenkin, M. E., and Saunders, S. M.: Photochemical ozone creation potentials for a large number of reactive
583 hydrocarbons under European conditions, *Atmos Environ*, 30, 181–199, [https://doi.org/https://doi.org/10.1016/1352-](https://doi.org/https://doi.org/10.1016/1352-2310(95)00303-G)
584 [2310\(95\)00303-G](https://doi.org/https://doi.org/10.1016/1352-2310(95)00303-G), 1996.
- 585
- 586 Donahue, N. M., Robinson, A. L., Stanier, C. O., and Pandis, S. N.: Coupled partitioning, dilution, and chemical aging of
587 semivolatile organics, *Environ Sci Technol*, 40, 2635–2643, <https://doi.org/10.1021/es052297c>, 2006.
- 588
- 589 Franco, B., Blumenstock, T., Cho, C., Clarisse, L., Clerbaux, C., Coheur, P.-F., de Mazière, M., de Smedt, I., Dorn, H.-P.,
590 Emmerichs, T., Fuchs, H., Gkatzelis, G., Griffith, D. W. T., Gromov, S., Hannigan, J. W., Hase, F., Hohaus, T., Jones, N.,



591 Kerkweg, A., Kiendler-Scharr, A., Lutsch, E., Mahieu, E., Novelli, A., Ortega, I., Paton-Walsh, C., Pommier, M., Pozzer, A.,
592 Reimer, D., Rosanka, S., Sander, R., Schneider, M., Strong, K., Tillmann, R., van Roozendaal, M., Vereecken, L., Vigouroux,
593 C., Wahner, A., and Taraborrelli, D.: Ubiquitous atmospheric production of organic acids mediated by cloud droplets, *Nature*,
594 593, 233–237, <https://doi.org/10.1038/s41586-021-03462-x>, 2021.

595

596 Friedman, B. and Farmer, D. K.: SOA and gas phase organic acid yields from the sequential photooxidation of seven
597 monoterpenes, *Atmos Environ*, 187, 335–345, [https://doi.org/https://doi.org/10.1016/j.atmosenv.2018.06.003](https://doi.org/10.1016/j.atmosenv.2018.06.003), 2018.

598

599 Fu, Z., Xie, H.-B., Elm, J., Guo, X., Fu, Z., and Chen, J.: Formation of Low-Volatile Products and Unexpected High
600 Formaldehyde Yield from the Atmospheric Oxidation of Methylsiloxanes, *Environ Sci Technol*, 54, 7136–7145,
601 <https://doi.org/10.1021/acs.est.0c01090>, 2020.

602

603 Gkatzelis, G. I., Coggon, M. M., McDonald, B. C., Peischl, J., Aikin, K. C., Gilman, J. B., Trainer, M., and Warneke, C.:
604 Identifying Volatile Chemical Product Tracer Compounds in U.S. Cities, *Environ Sci Technol*, 55, 188–199,
605 <https://doi.org/10.1021/acs.est.0c05467>, 2021.

606

607 De Gouw, J. and Warneke, C.: Measurements of volatile organic compounds in the earth's atmosphere using proton-transfer-
608 reaction mass spectrometry, *Mass Spectrom Rev*, 26, 223–257, [https://doi.org/https://doi.org/10.1002/mas.20119](https://doi.org/10.1002/mas.20119), 2007.

609

610 De Gouw, J., Warneke, C., Karl, T., Eerdekens, G., van der Veen, C., and Fall, R.: Sensitivity and specificity of atmospheric
611 trace gas detection by proton-transfer-reaction mass spectrometry, *Int J Mass Spectrom*, 223–224, 365–382,
612 [https://doi.org/https://doi.org/10.1016/S1387-3806\(02\)00926-0](https://doi.org/10.1016/S1387-3806(02)00926-0), 2003.

613

614 Graiver, D., Farminer, K. W., and Narayan, R.: A Review of the Fate and Effects of Silicones in the Environment, *J Polym*
615 *Environ*, 11, 129–136, <https://doi.org/10.1023/A:1026056129717>, 2003.

616

617 Han, C., Yang, H., Li, K., Lee, P., Liggio, J., Leithead, A., and Li, S.-M.: Secondary organic aerosols from OH oxidation of
618 cyclic volatile methyl siloxanes as an important Si source in the atmosphere, *Atmos Chem Phys*, 22, 10827–10839,
619 <https://doi.org/10.5194/acp-22-10827-2022>, 2022.

620

621 Hazra, M. K., Francisco, J. S., and Sinha, A.: Hydrolysis of Glyoxal in Water-Restricted Environments: Formation of Organic
622 Aerosol Precursors through Formic Acid Catalysis, *J Phys Chem A*, 118, 4095–4105, <https://doi.org/10.1021/jp502126m>,
623 2014.

624



- 625 Horii, Y., Nojiri, K., Minomo, K., Motegi, M., and Kannan, K.: Volatile methylsiloxanes in sewage treatment plants in Saitama,
626 Japan: Mass distribution and emissions, *Chemosphere*, 233, 677–686,
627 <https://doi.org/https://doi.org/10.1016/j.chemosphere.2019.05.247>, 2019.
628
- 629 Howard, P. H. and Muir, D. C. G.: Identifying New Persistent and Bioaccumulative Organics Among Chemicals in Commerce,
630 *Environ Sci Technol*, 44, 2277–2285, <https://doi.org/10.1021/es903383a>, 2010.
631
- 632 Isaacman-VanWertz, G., Massoli, P., O’Brien, R., Lim, C., Franklin, J. P., Moss, J. A., Hunter, J. F., Nowak, J. B.,
633 Canagaratna, M. R., Misztal, P. K., Arata, C., Roscioli, J. R., Herndon, S. T., Onasch, T. B., Lambe, A. T., Jayne, J. T., Su, L.,
634 Knopf, D. A., Goldstein, A. H., Worsnop, D. R., and Kroll, J. H.: Chemical evolution of atmospheric organic carbon over
635 multiple generations of oxidation, *Nat Chem*, 10, 462–468, <https://doi.org/10.1038/s41557-018-0002-2>, 2018.
636
- 637 Janecek, N. J., Marek, R. F., Bryngelson, N., Singh, A., Bullard, R. L., Brune, W. H., and Stanier, C. O.: Physical properties
638 of secondary photochemical aerosol from OH oxidation of a cyclic siloxane, *Atmos Chem Phys*, 19, 1649–1664,
639 <https://doi.org/10.5194/acp-19-1649-2019>, 2019.
640
- 641 Jordan, A., Haidacher, S., Hanel, G., Hartungen, E., Märk, L., Seehauser, H., Schottkowsky, R., Sulzer, P., and Märk, T. D.:
642 A high resolution and high sensitivity proton-transfer-reaction time-of-flight mass spectrometer (PTR-TOF-MS), *Int J Mass*
643 *Spectrom*, 286, 122–128, <https://doi.org/https://doi.org/10.1016/j.ijms.2009.07.005>, 2009.
644
- 645 Kaikiti, C., Stylianou, M., and Agapiou, A.: TD-GC/MS analysis of indoor air pollutants (VOCs, PM) in hair salons,
646 *Chemosphere*, 294, 133691, <https://doi.org/https://doi.org/10.1016/j.chemosphere.2022.133691>, 2022.
647
- 648 Kang, E., Root, M. J., Toohey, D. W., and Brune, W. H.: Introducing the concept of Potential Aerosol Mass (PAM), *Atmos*
649 *Chem Phys*, 7, 5727–5744, <https://doi.org/10.5194/acp-7-5727-2007>, 2007.
650
- 651 Katz, E. F., Lunderberg, D. M., Brown, W. L., Day, D. A., Jimenez, J. L., Nazaroff, W. W., Goldstein, A. H., and DeCarlo, P.
652 F.: Large Emissions of Low-Volatility Siloxanes during Residential Oven Use, *Environ Sci Technol Lett*, 8, 519–524,
653 <https://doi.org/10.1021/acs.estlett.1c00433>, 2021.
654
- 655 Kessler, S. H., Nah, T., Daumit, K. E., Smith, J. D., Leone, S. R., Kolb, C. E., Worsnop, D. R., Wilson, K. R., and Kroll, J. H.:
656 OH-Initiated Heterogeneous Aging of Highly Oxidized Organic Aerosol, *J Phys Chem A*, 116, 6358–6365,
657 <https://doi.org/10.1021/jp212131m>, 2012.
658



- 659 Kim, J. and Xu, S.: Quantitative structure-reactivity relationships of hydroxyl radical rate constants for linear and cyclic volatile
660 methylsiloxanes, *Environ Toxicol Chem*, 36, 3240–3245, <https://doi.org/10.1002/etc.3914>, 2017.
- 661
- 662 Kroll, J. H., Lim, C. Y., Kessler, S. H., and Wilson, K. R.: Heterogeneous Oxidation of Atmospheric Organic Aerosol: Kinetics
663 of Changes to the Amount and Oxidation State of Particle-Phase Organic Carbon, *J Phys Chem A*, 119, 10767–10783,
664 <https://doi.org/10.1021/acs.jpca.5b06946>, 2015.
- 665
- 666 Lee, S., Moon, H.-B., Song, G.-J., Ra, K., Lee, W.-C., and Kannan, K.: A nationwide survey and emission estimates of cyclic
667 and linear siloxanes through sludge from wastewater treatment plants in Korea, *Science of The Total Environment*, 497–498,
668 106–112, <https://doi.org/10.1016/j.scitotenv.2014.07.083>, 2014.
- 669
- 670 Lei, Y. D., Wania, F., and Mathers, D.: Temperature-Dependent Vapor Pressure of Selected Cyclic and Linear
671 Polydimethylsiloxane Oligomers, *J Chem Eng Data*, 55, 5868–5873, <https://doi.org/10.1021/je100835n>, 2010.
- 672
- 673 Link, M. F., Nguyen, T. B., Bates, K., Müller, J.-F., and Farmer, D. K.: Can Isoprene Oxidation Explain High Concentrations
674 of Atmospheric Formic and Acetic Acid over Forests?, *ACS Earth Space Chem*, 4, 730–740,
675 <https://doi.org/10.1021/acsearthspacechem.0c00010>, 2020.
- 676
- 677 Lu, D., Tan, J., Yang, X., Sun, X., Liu, Q., and Jiang, G.: Unraveling the role of silicon in atmospheric aerosol secondary
678 formation: a new conservative tracer for aerosol chemistry, *Atmos Chem Phys*, 19, 2861–2870, <https://doi.org/10.5194/acp-19-2861-2019>, 2019.
- 679
- 680
- 681 Mao, J., Ren, X., Brune, W. H., Olson, J. R., Crawford, J. H., Fried, A., Huey, L. G., Cohen, R. C., Heikes, B., Singh, H. B.,
682 Blake, D. R., Sachse, G. W., Diskin, G. S., Hall, S. R., and Shetter, R. E.: Airborne measurement of OH reactivity during
683 INTEX-B, *Atmos Chem Phys*, 9, 163–173, <https://doi.org/10.5194/acp-9-163-2009>, 2009.
- 684
- 685 Meng, T., Su, S., Cheng, J., Zhong, F., and Tang, Z.: Methylsiloxanes in street dust from Hefei, China: Distribution, sources,
686 and human exposure, *Environ Res*, 201, 111513, <https://doi.org/10.1016/j.envres.2021.111513>, 2021.
- 687
- 688 Milani, A., Al-Naiema, I. M., and Stone, E. A.: Detection of a secondary organic aerosol tracer derived from personal care
689 products, *Atmos Environ*, 246, 118078, <https://doi.org/10.1016/j.atmosenv.2020.118078>, 2021.
- 690
- 691 Millet, D. B., Jacob, D. J., Turquety, S., Hudman, R. C., Wu, S., Fried, A., Walega, J., Heikes, B. G., Blake, D. R., Singh, H.
692 B., Anderson, B. E., and Clarke, A. D.: Formaldehyde distribution over North America: Implications for satellite retrievals of



- 693 formaldehyde columns and isoprene emission, *Journal of Geophysical Research: Atmospheres*, 111,
694 <https://doi.org/https://doi.org/10.1029/2005JD006853>, 2006.
- 695
- 696 Millet, D. B., Baasandorj, M., Farmer, D. K., Thornton, J. A., Baumann, K., Brophy, P., Chaliyakunnel, S., de Gouw, J. A.,
697 Graus, M., Hu, L., Koss, A., Lee, B. H., Lopez-Hilfiker, F. D., Neuman, J. A., Paulot, F., Peischl, J., Pollack, I. B., Ryerson,
698 T. B., Warneke, C., Williams, B. J., and Xu, J.: A large and ubiquitous source of atmospheric formic acid, *Atmos Chem Phys*,
699 15, 6283–6304, <https://doi.org/10.5194/acp-15-6283-2015>, 2015.
- 700
- 701 Müller, M., Mikoviny, T., and Wisthaler, A.: Detector aging induced mass discrimination and non-linearity effects in PTR-
702 ToF-MS, *Int J Mass Spectrom*, 365–366, 93–97, <https://doi.org/https://doi.org/10.1016/j.ijms.2013.12.008>, 2014.
- 703
- 704 Newland, M. J., Bryant, D. J., Dunmore, R. E., Bannan, T. J., Acton, W. J. F., Langford, B., Hopkins, J. R., Squires, F. A.,
705 Dixon, W., Drysdale, W. S., Ivatt, P. D., Evans, M. J., Edwards, P. M., Whalley, L. K., Heard, D. E., Slater, E. J., Woodward-
706 Massey, R., Ye, C., Mehra, A., Worrall, S. D., Bacak, A., Coe, H., Percival, C. J., Hewitt, C. N., Lee, J. D., Cui, T., Surratt, J.
707 D., Wang, X., Lewis, A. C., Rickard, A. R., and Hamilton, J. F.: Low-NO atmospheric oxidation pathways in a polluted
708 megacity, *Atmos Chem Phys*, 21, 1613–1625, <https://doi.org/10.5194/acp-21-1613-2021>, 2021.
- 709
- 710 Odum, J. R., Hoffmann, T., Bowman, F., Collins, D., Flagan, R. C., and Seinfeld, J. H.: Gas/Particle Partitioning and Secondary
711 Organic Aerosol Yields, *Environ Sci Technol*, 30, 2580–2585, <https://doi.org/10.1021/es950943+>, 1996.
- 712
- 713 Peng, Z. and Jimenez, J. L.: Radical chemistry in oxidation flow reactors for atmospheric chemistry research, *Chem. Soc. Rev.*,
714 49, 2570–2616, <https://doi.org/10.1039/C9CS00766K>, 2020.
- 715
- 716 Peng, Z., Lee-Taylor, J., Orlando, J. J., Tyndall, G. S., and Jimenez, J. L.: Organic peroxy radical chemistry in oxidation flow
717 reactors and environmental chambers and their atmospheric relevance, *Atmos Chem Phys*, 19, 813–834,
718 <https://doi.org/10.5194/acp-19-813-2019>, 2019.
- 719
- 720 Pennington, E. A., Seltzer, K. M., Murphy, B. N., Qin, M., Seinfeld, J. H., and Pye, H. O. T.: Modeling secondary organic
721 aerosol formation from volatile chemical products, *Atmos Chem Phys*, 21, 18247–18261, [https://doi.org/10.5194/acp-21-](https://doi.org/10.5194/acp-21-18247-2021)
722 18247-2021, 2021.
- 723
- 724 Piel, F., Müller, M., Winkler, K., af Sättra, J., and Wisthaler, A.: Introducing the extended volatility range proton-transfer-
725 reaction mass spectrometer (EVR PTR-MS), *Atmos Meas Tech*, 14, 1355–1363, <https://doi.org/10.5194/amt-14-1355-2021>,
726 2021.



727
728 Porter, W. C., Jimenez, J. L., and Barsanti, K. C.: Quantifying Atmospheric Parameter Ranges for Ambient Secondary Organic
729 Aerosol Formation, *ACS Earth Space Chem*, 5, 2380–2397, <https://doi.org/10.1021/acsearthspacechem.1c00090>, 2021.
730
731 Pöschl, U., Rudich, Y., and Ammann, M.: Kinetic model framework for aerosol and cloud surface chemistry and gas-particle
732 interactions – Part 1: General equations, parameters, and terminology, *Atmos Chem Phys*, 7, 5989–6023,
733 <https://doi.org/10.5194/acp-7-5989-2007>, 2007.
734
735 Robinson, A. L., Donahue, N. M., Shrivastava, M. K., Weitkamp, E. A., Sage, A. M., Grieshop, A. P., Lane, T. E., Pierce, J.
736 R., and Pandis, S. N.: Rethinking Organic Aerosols: Semivolatile Emissions and Photochemical Aging, *Science* (1979), 315,
737 1259–1262, <https://doi.org/10.1126/science.1133061>, 2007.
738
739 Rücker, C. and Kümmerer, K.: Environmental Chemistry of Organosiloxanes, *Chem Rev*, 115, 466–524,
740 <https://doi.org/10.1021/cr500319v>, 2015.
741
742 Safron, A., Strandell, M., Kierkegaard, A., and Macleod, M.: Rate Constants and Activation Energies for Gas-Phase Reactions
743 of Three Cyclic Volatile Methyl Siloxanes with the Hydroxyl Radical, *Int J Chem Kinet*, 47, 420–428,
744 <https://doi.org/https://doi.org/10.1002/kin.20919>, 2015.
745
746 Schweigkofler, M. and Niessner, R.: Determination of Siloxanes and VOC in Landfill Gas and Sewage Gas by Canister
747 Sampling and GC-MS/AES Analysis, *Environ Sci Technol*, 33, 3680–3685, <https://doi.org/10.1021/es9902569>, 1999.
748
749 Seltzer, K. M., Pennington, E., Rao, V., Murphy, B. N., Strum, M., Isaacs, K. K., and Pye, H. O. T.: Reactive organic carbon
750 emissions from volatile chemical products, *Atmos Chem Phys*, 21, 5079–5100, <https://doi.org/10.5194/acp-21-5079-2021>,
751 2021a.
752
753 Seltzer, K. M., Murphy, B. N., Pennington, E. A., Allen, C., Talgo, K., and Pye, H. O. T.: Volatile Chemical Product
754 Enhancements to Criteria Pollutants in the United States, *Environ Sci Technol*, <https://doi.org/10.1021/acs.est.1c04298>, 2021b.
755
756 Sommerlade, R., Parlar, H., Wrobel, D., and Kochs, P.: Product analysis and kinetics of the gas-phase reactions of selected
757 organosilicon compounds with OH radicals using a smog chamber-mass spectrometer system, *Environ Sci Technol*, 27, 2435–
758 2440, <https://doi.org/10.1021/es00048a019>, 1993.
759



- 760 Sommers, J. M., Stroud, C. A., Adam, M. G., O'Brien, J., Brook, J. R., Hayden, K., Lee, A. K. Y., Li, K., Liggio, J., Mihele,
761 C., Mittermeier, R. L., Stevens, R. G., Wolde, M., Zuend, A., and Hayes, P. L.: Evaluating SOA formation from different
762 sources of semi- and intermediate-volatility organic compounds from the Athabasca oil sands, *Environmental Science:*
763 *Atmospheres*, 2, 469–490, <https://doi.org/10.1039/D1EA00053E>, 2022.
- 764
- 765 Song, K., Gong, Y., Guo, S., Lv, D., Wang, H., Wan, Z., Yu, Y., Tang, R., Li, T., Tan, R., Zhu, W., Shen, R., and Lu, S.:
766 Investigation of partition coefficients and fingerprints of atmospheric gas- and particle-phase intermediate volatility and semi-
767 volatile organic compounds using pixel-based approaches, *J Chromatogr A*, 1665, 462808,
768 <https://doi.org/https://doi.org/10.1016/j.chroma.2022.462808>, 2022.
- 769
- 770 Spivack, J. L., Pohl, E. R., and Kochs, P.: Organoalkoxysilanes, Organosilanols, and Organosiloxanols, in: *Organosilicon*
771 *Materials*, edited by: Chandra, G., Springer Berlin Heidelberg, Berlin, Heidelberg, 105–135, [https://doi.org/10.1007/978-3-](https://doi.org/10.1007/978-3-540-68331-5_5)
772 [540-68331-5_5](https://doi.org/10.1007/978-3-540-68331-5_5), 1997.
- 773
- 774 Stevens, C.: Environmental degradation pathways for the breakdown of polydimethylsiloxanes, *J Inorg Biochem*, 69, 203–
775 207, [https://doi.org/https://doi.org/10.1016/S0162-0134\(97\)10019-8](https://doi.org/https://doi.org/10.1016/S0162-0134(97)10019-8), 1998.
- 776
- 777 Tang, X., Misztal, P. K., Nazaroff, W. W., and Goldstein, A. H.: Siloxanes Are the Most Abundant Volatile Organic Compound
778 Emitted from Engineering Students in a Classroom, *Environ Sci Technol Lett*, 2, 303–307,
779 <https://doi.org/10.1021/acs.estlett.5b00256>, 2015.
- 780
- 781 Tansel, B. and Surita, S. C.: Historical and projected trends of siloxane use in consumer products, associated impacts on
782 municipal solid waste and landfill gas utilization, *International Journal of Environmental Science and Technology*, 14, 795–
783 802, <https://doi.org/10.1007/s13762-016-1186-x>, 2017.
- 784
- 785 Tran, T. M. and Kannan, K.: Occurrence of cyclic and linear siloxanes in indoor air from Albany, New York, USA, and its
786 implications for inhalation exposure, *Science of The Total Environment*, 511, 138–144,
787 <https://doi.org/https://doi.org/10.1016/j.scitotenv.2014.12.022>, 2015.
- 788
- 789 TSI Inc.: MEASURING NANOPARTICLE SIZE DISTRIBUTIONS IN REAL-TIME: KEY FACTORS FOR ACCURACY,
790 2012.
- 791
- 792 Wang, N., Ernle, L., Bekö, G., Wargocki, P., and Williams, J.: Emission Rates of Volatile Organic Compounds from Humans,
793 *Environ Sci Technol*, 56, 4838–4848, <https://doi.org/10.1021/acs.est.1c08764>, 2022.



794

795 Whelan, M. J. and Kim, J.: Application of multimedia models for understanding the environmental behavior of volatile
796 methylsiloxanes: Fate, transport, and bioaccumulation, *Integr Environ Assess Manag*, n/a, 1–23,
797 <https://doi.org/https://doi.org/10.1002/ieam.4507>, 2021.

798

799 Whelan, M. J., Estrada, E., and van Egmond, R.: A modelling assessment of the atmospheric fate of volatile methyl siloxanes
800 and their reaction products, *Chemosphere*, 57, 1427–1437, <https://doi.org/https://doi.org/10.1016/j.chemosphere.2004.08.100>,
801 2004.

802

803 Wu, Y. and Johnston, M. V: Aerosol Formation from OH Oxidation of the Volatile Cyclic Methyl Siloxane (cVMS)
804 Decamethylcyclopentasiloxane, *Environ Sci Technol*, 51, 4445–4451, <https://doi.org/10.1021/acs.est.7b00655>, 2017.

805

806 Xiang, X., Liu, N., Xu, L., and Cai, Y.: Review of recent findings on occurrence and fates of siloxanes in environmental
807 compartments, *Ecotoxicol Environ Saf*, 224, 112631, <https://doi.org/https://doi.org/10.1016/j.ecoenv.2021.112631>, 2021.

808

809 Xiao, R., Zammit, I., Wei, Z., Hu, W.-P., MacLeod, M., and Spinney, R.: Kinetics and Mechanism of the Oxidation of Cyclic
810 Methylsiloxanes by Hydroxyl Radical in the Gas Phase: An Experimental and Theoretical Study, *Environ Sci Technol*, 49,
811 13322–13330, <https://doi.org/10.1021/acs.est.5b03744>, 2015.

812

813 Xu, J., Harrison, R. M., Song, C., Hou, S., Wei, L., Fu, P., Li, H., Li, W., and Shi, Z.: PM_{2.5}-bound silicon-containing
814 secondary organic aerosols (Si-SOA) in Beijing ambient air, *Chemosphere*, 288, 132377,
815 <https://doi.org/https://doi.org/10.1016/j.chemosphere.2021.132377>, 2022.

816

817 Xu, N. and Collins, D. R.: Design and characterization of a new oxidation flow reactor for laboratory and long-term ambient
818 studies, *Atmos Meas Tech*, 14, 2891–2906, <https://doi.org/10.5194/amt-14-2891-2021>, 2021.

819

820 Yu, S.: Role of organic acids (formic, acetic, pyruvic and oxalic) in the formation of cloud condensation nuclei (CCN): a
821 review, *Atmos Res*, 53, 185–217, [https://doi.org/https://doi.org/10.1016/S0169-8095\(00\)00037-5](https://doi.org/https://doi.org/10.1016/S0169-8095(00)00037-5), 2000.

822

823 Yuan, B., Veres, P. R., Warneke, C., Roberts, J. M., Gilman, J. B., Koss, A., Edwards, P. M., Graus, M., Kuster, W. C., Li, S.-
824 M., Wild, R. J., Brown, S. S., Dubé, W. P., Lerner, B. M., Williams, E. J., Johnson, J. E., Quinn, P. K., Bates, T. S., Lefer, B.,
825 Hayes, P. L., Jimenez, J. L., Weber, R. J., Zamora, R., Ervens, B., Millet, D. B., Rappenglück, B., and de Gouw, J. A.:
826 Investigation of secondary formation of formic acid: urban environment vs. oil and gas producing region, *Atmos. Chem. Phys.*,
827 15, 1975–1993, <https://doi.org/10.5194/acp-15-1975-2015>, 2015.



828

829 Zhao, B., Wang, S., Donahue, N. M., Chuang, W., Hildebrandt Ruiz, L., Ng, N. L., Wang, Y., and Hao, J.: Evaluation of One-
830 Dimensional and Two-Dimensional Volatility Basis Sets in Simulating the Aging of Secondary Organic Aerosol with Smog-
831 Chamber Experiments, *Environ Sci Technol*, 49, 2245–2254, <https://doi.org/10.1021/es5048914>, 2015.

832

833 Zhao, Z., Tolentino, R., Lee, J., Vuong, A., Yang, X., and Zhang, H.: Interfacial Dimerization by Organic Radical Reactions
834 during Heterogeneous Oxidative Aging of Oxygenated Organic Aerosols, *J Phys Chem A*, 123, 10782–10792,
835 <https://doi.org/10.1021/acs.jpca.9b10779>, 2019.

836

837

838

839

840

841

842

843

844

845

846

847

848

849

850

851

852

853

854

855

856

857

858

859

860

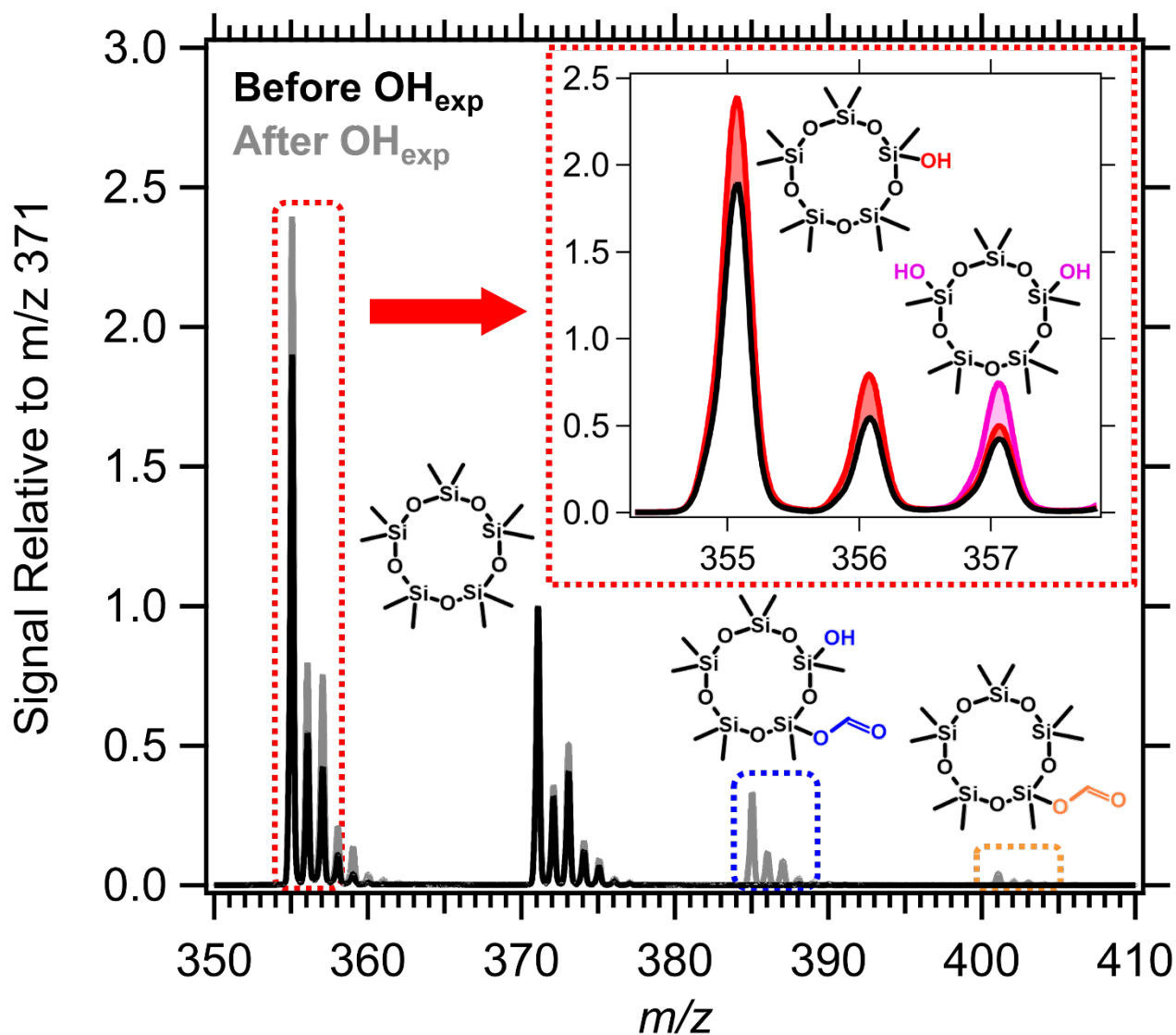


861 **Table 1. Summary of SOSiA mass yields (Y_{SOSiA}) with aerosol sampling line corrections assuming $\rho_{\text{SOSiA}} = 1.07 \text{ g cm}^{-3}$ for all**
 862 **experiments. $[\text{H}_2\text{O}]$ is the molar mixing ratio of H_2O in air. For C_{OA} and $[\text{D}_5]$, the errors are the standard deviation of the data points**
 863 **averaged, while for Y_{SOSiA} , they are calculated with error propagation. For reference, at 25 °C and 1 atm, 1 ppb of D_5 is $\sim 15 \mu\text{g m}^{-3}$**
 864 **and one day equivalent of OH_{exp} is $\sim 1.3 \times 10^{11} \text{ s cm}^{-3}$ at a daily $[\text{OH}]_{\text{avg}}$ of $1.5 \times 10^6 \text{ cm}^{-3}$.**

Experiment	Y_{SOSiA} (%)	$[\text{H}_2\text{O}]$ (%)	C_{OA} ($\mu\text{g m}^{-3}$)	OH_{exp} (s cm^{-3})	$[\text{OH}]$ (cm^{-3})	$[\text{D}_5]_0$ (ppb)	$1 - [\text{D}_5]_{\text{final}}/[\text{D}_5]_0$
1	5.9 ± 0.9	0.892	10.5 ± 0.7	1.73×10^{11}	9.59×10^8	43.4 ± 1.3	0.292
2	4.9 ± 0.6	0.828	19.0 ± 0.6	1.90×10^{11}	1.06×10^9	85.7 ± 2.5	0.316
3	3.3 ± 0.6	0.742	17.7 ± 0.5	1.26×10^{11}	6.99×10^8	165.8 ± 4.5	0.222
4	19.5 ± 1.5	1.95	75.2 ± 1.9	4.66×10^{11}	2.59×10^9	44.0 ± 1.7	0.606
5	29.3 ± 2.7	2.06	179.2 ± 3.1	3.80×10^{11}	2.11×10^9	78.3 ± 3.2	0.532
6	26.5 ± 1.8	2.09	286.2 ± 7.1	3.12×10^{11}	1.73×10^9	157.8 ± 3.6	0.464
7	8.6 ± 0.5	0.733	36.8 ± 1.3	5.76×10^{11}	3.20×10^9	43.8 ± 1.3	0.684
8	18.6 ± 1.7	0.736	118.6 ± 5.6	4.00×10^{11}	2.22×10^9	78.9 ± 3.2	0.550
9	21.8 ± 1.1	0.797	304.5 ± 2.8	4.19×10^{11}	2.33×10^9	166.8 ± 4.1	0.567
10	39.8 ± 2.2	1.93	212.9 ± 8.1	9.01×10^{11}	5.00×10^9	43.8 ± 1.4	0.835
11	47.4 ± 1.9	2.08	420.2 ± 3.0	7.78×10^{11}	4.32×10^9	76.5 ± 2.2	0.789
12	54.0 ± 2.4	2.15	965.7 ± 25	7.39×10^{11}	4.10×10^9	156.9 ± 3.9	0.772
13	4.7 ± 1.7	0.712	3.9 ± 0.3	8.70×10^{10}	7.25×10^8	37.9 ± 1.6	0.160
14	1.9 ± 0.4	0.718	4.1 ± 0.3	1.09×10^{11}	9.10×10^8	80.8 ± 2.3	0.196
15	1.1 ± 0.3	0.704	3.7 ± 0.7	8.29×10^{10}	6.91×10^8	162.8 ± 4.9	0.153

865

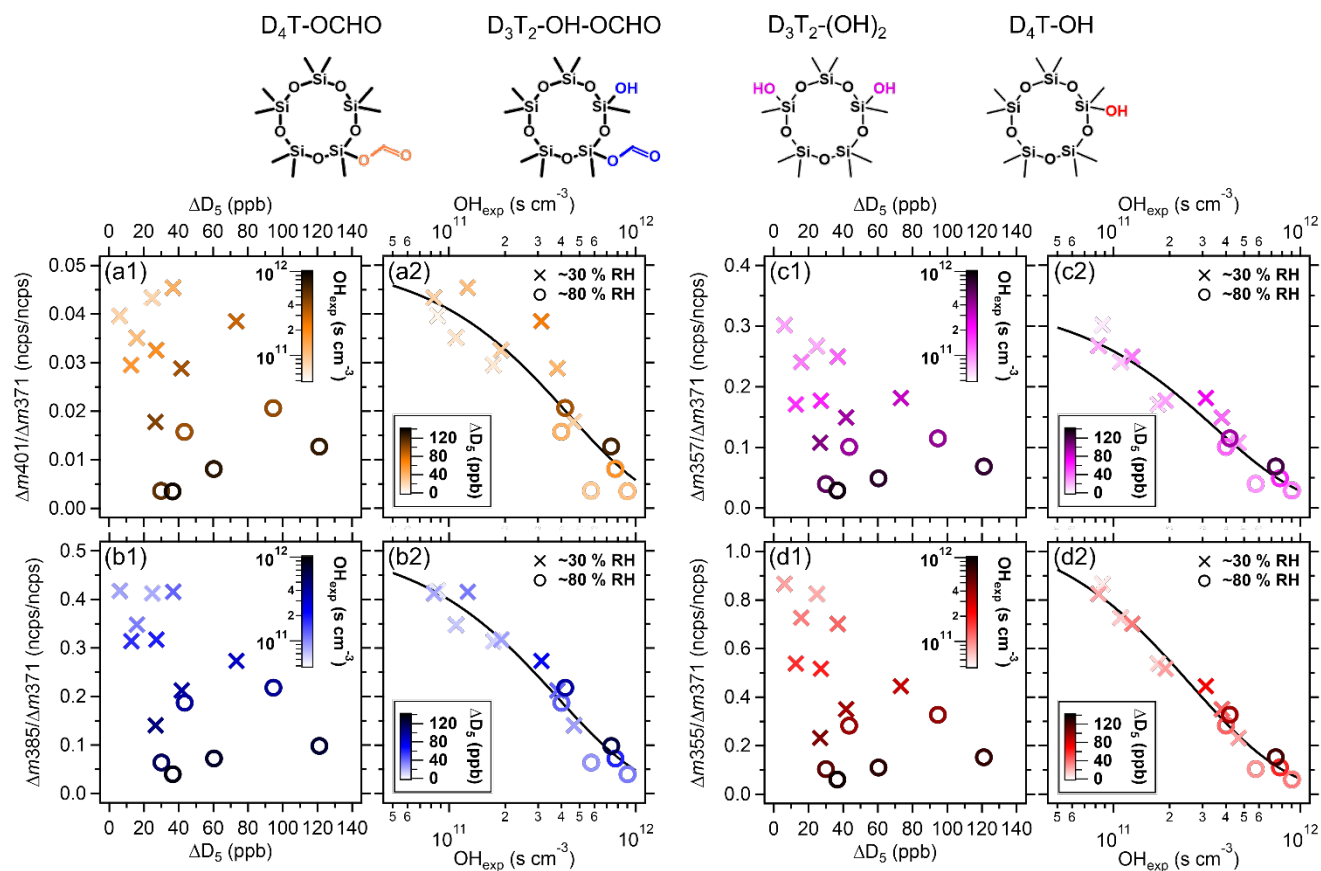
866



867

868 **Figure 1. Example PTR-MS mass spectra from experiment 12 and proposed VOP ions.** The signal intensities, before (black) and after
 869 (grey) oxidation, are each normalized to the signal intensity of the D_5 ion at m/z 371, which is set to 1. The multifunctional species (blue,
 870 pink) are expected to be formed through multiple steps of OH-oxidation. The red and pink areas in the inset each refer to the enhancement
 871 in signal attributed to $\text{D}_4\text{T-OH}$ and $\text{D}_3\text{T}_2\text{-(OH)}_2$ over that of the $-\text{CH}_3$ fragment of D_5 and isotope signals, respectively.

872

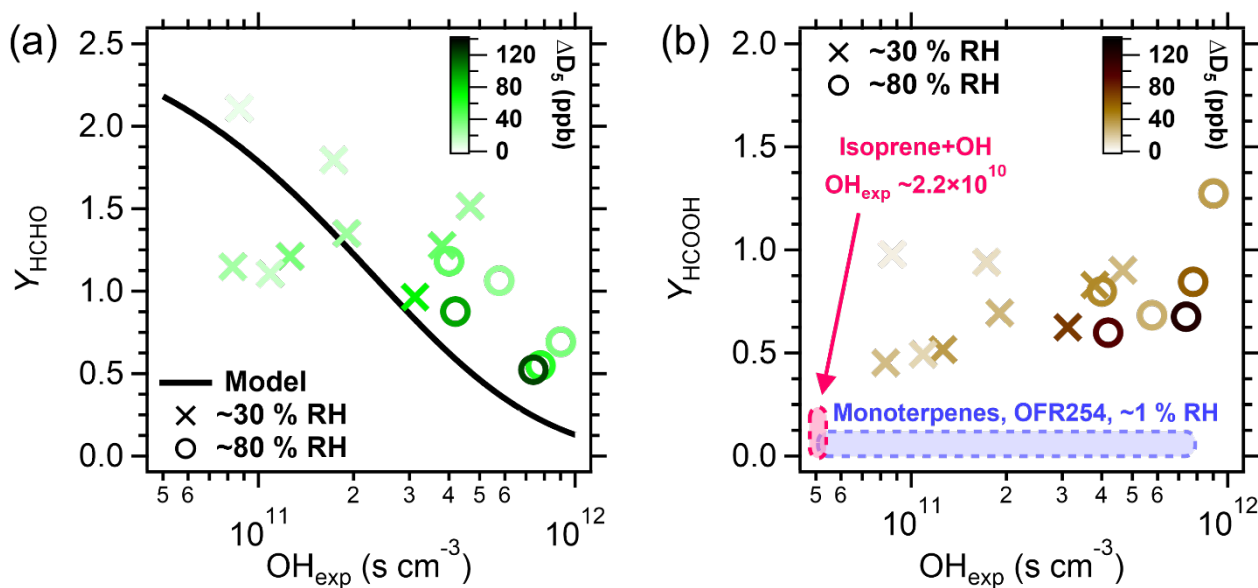


873

874 **Figure 2. Relative molar yields of selected VOP.** Molar yields as a function of OH_{exp} and D_5 consumed in experiments for (a1, a2) $D_4T-OCHO$,
 875 $D_3T_2-OH-OCHO$, (b1, b2) $D_3T_2-OH-OCHO$, (c1, c2) $D_3T_2-(OH)_2$, and (d1, d2) D_4T-OH . We did not have a calibration for the suspected VOP, so the
 876 y-axes are relative molar yields (ncps/ncps) calculated with the change in signal attributed to each VOP and that of D_5 at m/z 371. The
 877 relative molar yields decrease with OH_{exp} , which is used to fit their OH -oxidation rate coefficients and γ_i (black lines).

878

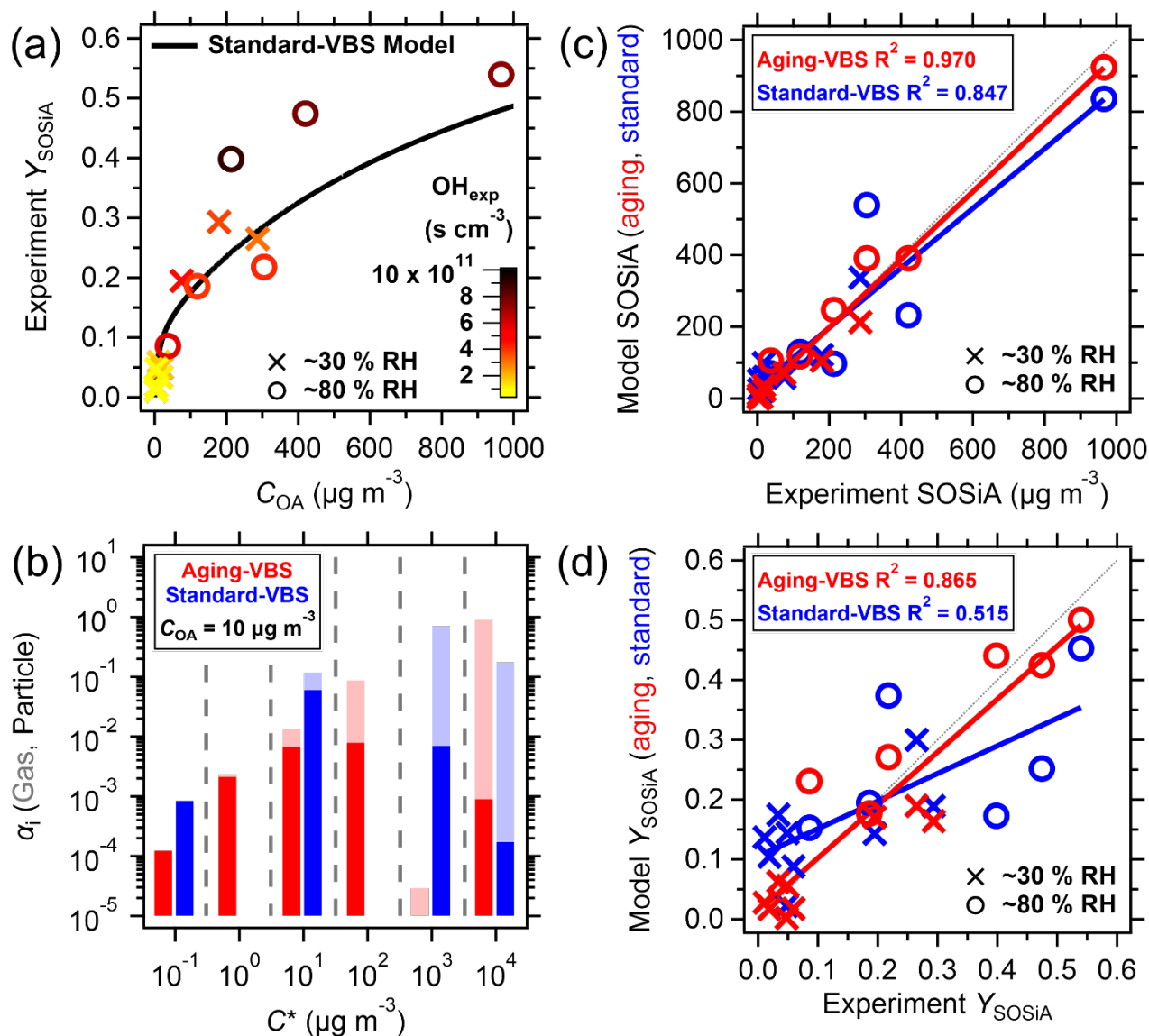
879



880

881 **Figure 3. Experimental molar yields of selected VOP: (a) HCHO and (b) HCOOH as functions of OH_{exp} .** The blue shaded area in (b)
 882 is the range of Y_{HCOOH} (< 10 %) measured by Friedman and Farmer (2018) with monoterpenes under low RH and low NO_x conditions. The
 883 pink shaded area refers to Y_{HCOOH} from isoprene + OH chamber experiments (Link et al., 2020) at lower OH_{exp} .

884



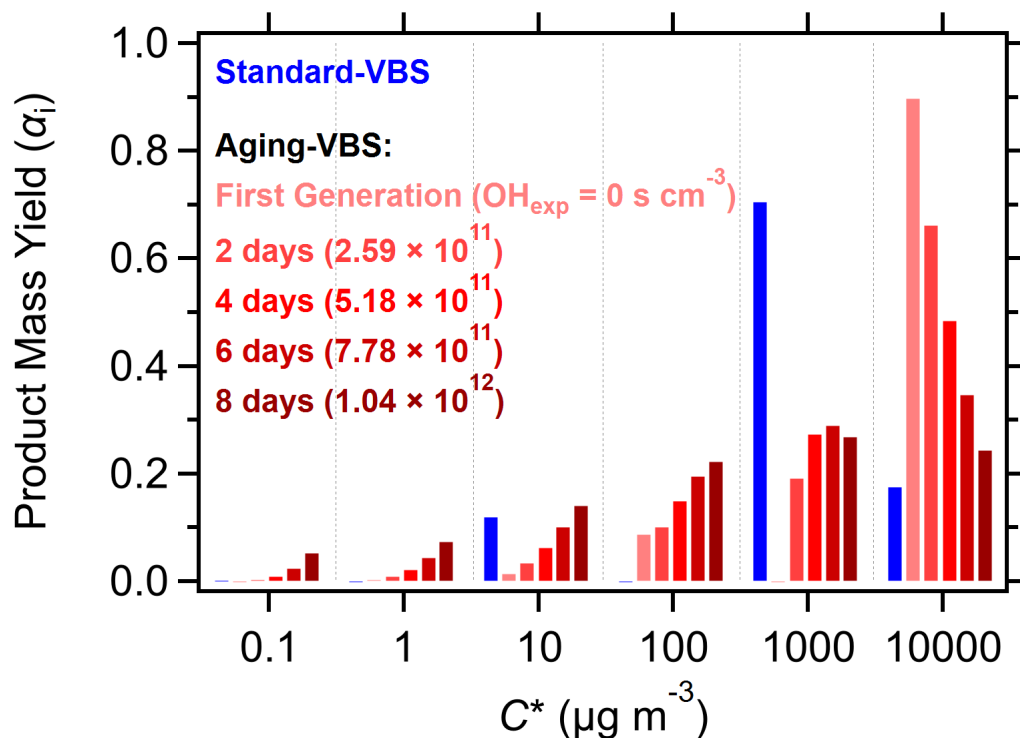
885

886 **Figure 4. Application of standard-VBS and aging-VBS models to experimental data.** (a) Y_{SOSiA} as a function of C_{OA} , where the Y_{SOSiA}
 887 appears to be correlated with OH_{exp} . (b) VBS product mass yields for each volatility bin. For the aging-VBS, the values are those of the first-
 888 generation products. (c) Comparison of SOSiA mass concentrations from the aging-VBS and standard-VBS models against measurements.
 889 (d) Comparison of Y_{SOSiA} from the aging-VBS and standard-VBS models against measurements, where the aging-VBS model has a higher
 890 R^2 .

891

892

893



894

895 **Figure 5. Evolution of the volatility distribution with OH_{exp} .** The standard-VBS model parameterization (blue bars) is dominated by the
 896 $C^* = 1\,000 \mu\text{g m}^{-3}$ volatility bin. In the aging-VBS model, the first-generation volatility distribution is dominated by the highest volatility
 897 bin ($C^* = 10\,000 \mu\text{g m}^{-3}$) but decreases with increasing OH_{exp} (red bars).

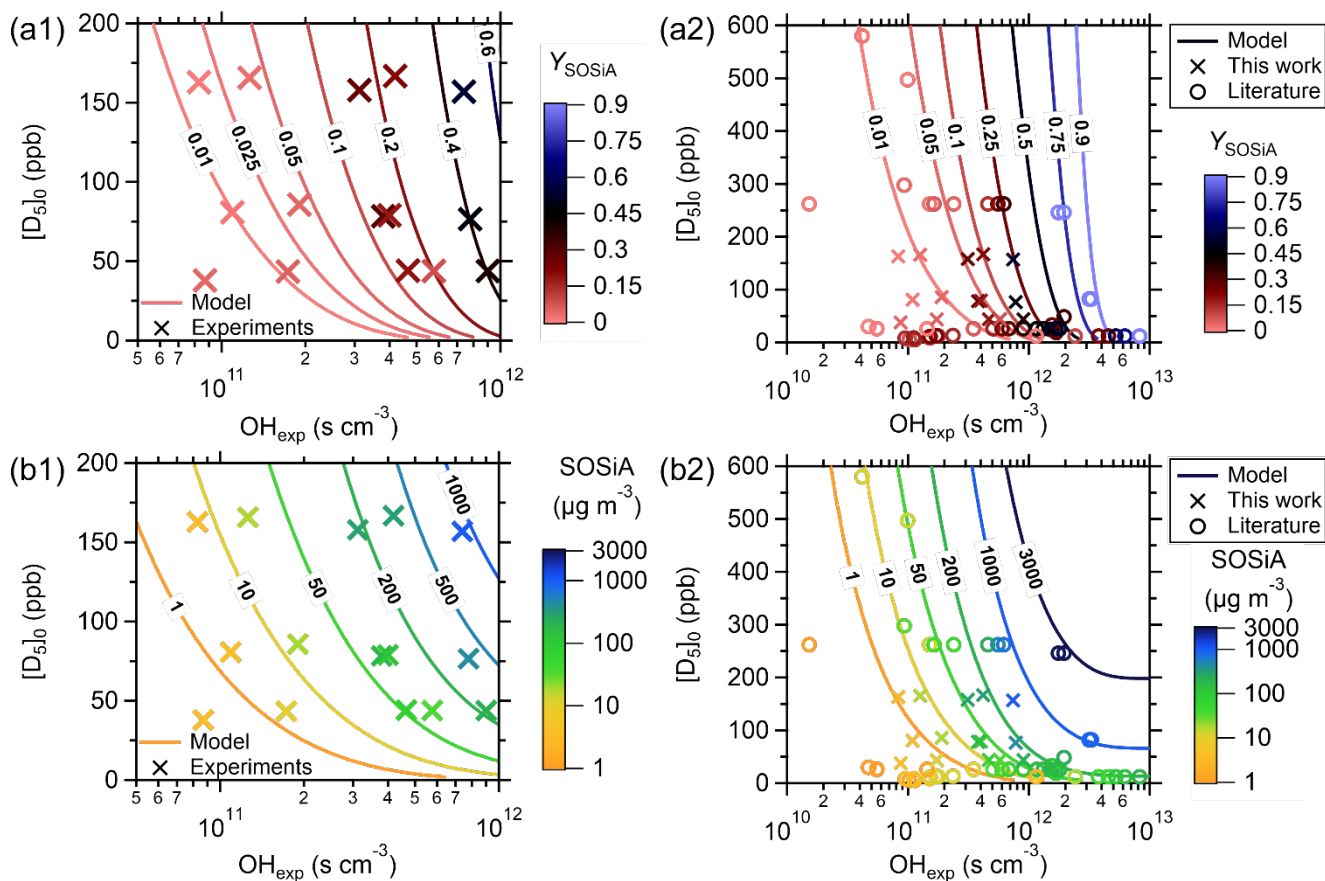
898

899

900

901

902



903

904 **Figure 6. Comparison of experiments, model results, and literature values.** (a) Y_{SOSiA} and (b) $SOSiA$ mass concentrations as a function
 905 of $[D_5]_0$ and OH_{exp} . The aging VBS-model is fit using experimental data from (1) this study and (2) including those in the literature. $SOSiA$
 906 formation generally increases with $[D_5]_0$ and OH_{exp} . The aging-VBS can capture the broad range of Y_{SOSiA} reported in the literature.